CHARGE CARRIER TRANSPORT IN CONJUGATED POLYMERS

By

BRYAN E. WILSON

A THESIS PRESENTED TO THE GRADUATE SCHOOL
OF THE UNIVERSITY OF FLORIDA IN PARTIAL FULFILLMENT
OF THE REQUIREMENTS FOR THE DEGREE OF
MASTER OF SCIENCE

UNIVERSITY OF FLORIDA

2007

To my mother, Isabel. I work hard because she's worked harder.

ACKNOWLEDGMENTS

First, I thank my beautiful and wonderful Fiancée, Johanna Talcott, for organizing everything from my references to my work area. Without her, I'd still be digging through a pile of papers looking for the perfect reference. Also, I thank her for all those late night dinners while I spent hours isolated in the office working on this project. She has never given up hope that I would ever finish my thesis and without that, I may have already quit.

My parents of course deserve a lot of credit as well. Always trying to keep me focused on the bright side of things, my mother has provided continued support through the many challenges I personally faced while trying to complete this work. My father has also provided support and I'm forever thankful to him for being there for me and always willing to talk things over.

Many thanks to Dr. Reynolds and his research group in the Department of Chemistry at the University of Florida for providing all of the materials and some of the equipment to perform my research.

My interest in the field of electronic materials has its roots in my work at A&N Corporation in Williston, Florida. A&N provided the flexibility for me to attend graduate school while keeping my job as an R&D engineer. Special thanks to my former supervisor, Vern McCoy and to the Vaudreuil family for opening the door to so many opportunities.

Last, but definitely not least, I'd like to extend my sincere appreciation to Dr. Paul H. Holloway, my graduate research advisor. From the first moment I approached him about my interest in the graduate program at the Department of Materials Science and Engineering to the day before my thesis submission deadline, he has provided many hours of guidance and an infinite level of patience. When things got tough and I was ready to throw in the towel, Dr. Holloway always found ways to keep me in the game and always provided me with new ways of looking at my data and understanding my work.

Additionally, this work was funded in part by the U.S. Army Research Laboratory under contract W911-NF-04-200023 with additional sponsorship provided by the Air Force Office of Scientific Research.

TABLE OF CONTENTS

page

LIST OF TABLES

LIST OF FIGURES

LIST OF ABBREVIATIONS

Eg	bandgap
q	carrier charge
ν	carrier drift velocity
T_{tr}	carrier transit time
σ	conductivity
J	current density
J_x	current density in x direction
$\hbar$	Dirac's constant
d	distance between repeat units in polymer
E	electric field
m	electron mass
ΔE	energy change between bands
E_n	energy eigen values
E_{HOMO}	energy of highest occupied molecular orbital
E_{LUMO}	energy of lowest unoccupied molecular orbital
γ	field effect factor
d	film thickness
R_H	hall coefficient
E_y	hall field
W	hall film thickness
V_y	induced potential

k_n	k-value, as related to energy Eigen values
B_z	magnetic field in z-direction
μ	mobility
N	number of orbitals, number of repeat units
ε_o	permittivity of free space
h	Planck's constant
L	polymer chain length or infinite well length
n	quantized states, or number of free carriers
ε_r	relative permittivity
Tc	trap characteristic temperature
N_t	trap density
V	volts
Ψ	wave function

Abstract of Thesis Presented to the Graduate School
of the University of Florida in Partial Fulfillment of the
Requirements for the Degree of Master of Science

CHARGE CARRIER TRANSPORT IN CONJUGATED POLYMERS

By

Bryan E. Wilson

December 2007

Chair: Paul H. Holloway
Major: Materials Science and Engineering

Current-Voltage measurements and charge transport properties of poly(3-hexyl-thiophene) ("P3HT"), poly(3,4-propylenedioxythiophene) ("PProDOT") and poly(3,4-propylenedioxythiophene-diethylhexyloxy)-cyano-p-phenylenevinylene substituted with dodecyloxy chains on the phenylene ring ("PProH") films have been studied. The zero-field hole mobility (μ_h) was determined from current-voltage data by iterating curve fitting parameters in the space charge limited current model which was derived from Child's Law, also known as the Mott-Gurney Law. To measure hole mobility, hole only devices were constructed with indium-tin-oxide (ITO) anodes and gold cathodes (very large electron injection barrier) on a glass substrate. A hole transport layer of Poly(3,4-ethylene-dioxythiophene):poly(styrenesulfonate) ("PEDOT") was spin coated between the ITO and sample polymer film in order to reduce the energy barrier for injection of holes. The effects of spin coating speed on film thickness, and subsequently on the electronic properties of the materials was also investigated.

Device preparation in a glove box using an argon ambient with oxygen and water concentrations of <5 ppm was found to be critical for reproducible electrical data. Spin coating speeds of 700 – 1000 RPM for 30 seconds resulted in thin films ranging between 10-90 nm as measured by atomic force microscopy (AFM). Hole transport in films of PProH was space charge limited for voltages in the range of 0-5V, with mobilities of $1.6x10^{-6}$ cm^2/V-s. In contrast, hole transport in films of PProDOT was trap limited. The origins of the traps were speculated to be residual impurities and/or structural deformations.

CHAPTER 1
INTRODUCTION AND MOTIVATION

The increased use of organic and polymer light emitting diodes (OLEDs and PLEDs) in the solid state lighting and display industries is the motivating force for the research presented in this work. Currently, conversion of energy from fossil and nuclear fuels to electricity provides most of the energy required to artificially illuminate living and working environments. In a recent publication, the United States Energy Information Administration showed that the energy used to meet domestic residential and commercial lighting requirements in 2005 was 4.2 quadrillion BTUs [1]. However, because the currently available sources of light are inefficient, only about 30% of this total energy was used to actually produce light with the rest being wasted as heat [2]. The limited quantities and environmental impacts associated with the use of fossil fuel and nuclear energy points to decreasing the amount of wasted energy with the introduction of new lighting technologies utilizing efficient, emissive materials.

Coincidentally, the development of new emissive materials and new technologies in the display industry is also being investigated. Technologies such as the Cathode Ray Tube (CRT), Liquid Crystal Displays (LCDs) and Plasma Display Panels (PDPs) currently dominate the display market [3]. However, several factors have limited these technologies. For example, though the technology is currently the cheapest available, the bulkiness and weight of CRTs have excluded them from the popular flat panel market [3]. Also, viewing angle restrictions caused by the birefringence property of liquid

crystals in LCDs has caused the need for development of compensating technologies [3]. Finally, the high energy requirement of PDPs has limited this technology to static (i.e., non-portable) applications. The advantages of OLEDs are that they are easy to process, are characterized by low operating voltages and exhibit wide viewing angles and high contrast ratios. Furthermore, the mechanical properties of polymer films open the door to flexible display applications [4, 5].

Typically light emitting diodes are separated into two categories: inorganic (hereby referred to as LEDs) and organic (referred to as OLEDs). OLEDS may be further categorized as either small molecule (SMOLED) or conjugated polymer (PLED) devices. Devices based on inorganic materials are generally comprised of compound semiconductors such GaAs, GaP, AlGaAs, InGaP, GaAsP, SiC, ZnSe or InAlGaN. However, the technologies used to deposit these materials are similar to that utilized to fabricate silicon integrated circuits thereby making them relatively expensive [6]. On the other hand, while SMOLED technology may also take advantage of precision deposition technologies such as those requiring vacuum, depositing polymer materials for PLEDs is quite cheap as the material can be deposited from solution by spin coating, sometimes in ambient laboratory conditions.

In any OLED, emission of light requires electrical charge (electrons and holes) to be injected into the organic thin films, for the electrical charge to be transported in the material with minimum energy loss, and for the electrons and holes to recombine and emit light. The focus of this research is the charge transport properties, namely the hole mobility (μ_h), of a novel polymer material: poly(3,4-propylenedioxythiophene-diethylhexyloxy)-cyano-p-phenylene vinylene substituted with dodecyloxy chains on the

phenylene ring, referred to as PProH:CNP(MEH) or PProH for simplicity. Charge transport was measured as the current versus applied voltage as a function of processing and time. Spin-coating was investigated as an easy deposition method which allows the sample film thickness to be varied. The current transport is also correlated with changes in the film thickness.

This work describes relatively simple process for gaining insight to the charge transport properties of new polymer materials. By measuring and reporting hole transport properties of new materials, this work provides knowledge that may be used in the future to improve OLED based devices and their respective efficiencies.

In this thesis, a review of the literature in Chapter 2 provides a description of polymer based device physics, and electrical properties. The experimental procedures section, Chapter 3, includes a review of the processing methods and a description of characterization tools that were used to determine the hole-mobility from electrical properties. Chapter 4 contains the experimental results and comparison of electrical properties of devices utilizing films of PProh:CNP(MEH). Finally, Chapter 5 provides a summary and conclusions from the experimental results of this work as well as recommendations for future work.

CHAPTER 2
LITERATURE REVIEW

2.1 Introduction

The purpose of the study described in this thesis is to measure carrier transport properties in conducting, conjugated polymers. This was accomplished by comparing experimental data from current-voltage (I-V) measurements with the space-charge limited current (SCLC) or trap-limited current (TLC) models to extract the hole mobility (μ). The results from this work are useful for several applications, including those related to organic light emitting diode (OLED) applications with respect to charge balancing for efficient electron-hole recombination and photon emission. This chapter reviews background information which includes a brief history of the OLEDs, device architecture and operation, conducting polymer physics, and the modeling of carrier transport mobility.

2.2 Organic Light Emitting Diodes

2.2.1 History

Electroluminescence (EL) is the non-thermal generation of light resulting from the application of an electric field, and is accomplished by recombination of charge carriers of contrary sign (electrons and holes) that are injected into a semiconductor in the presence of an external circuit [6]. EL was demonstrated in organic materials in 1963. EL has been reported as first being observed from inorganic ZnS phosphor powder by Destriau et al. in 1936 [7]. Recently however, some have credited the earlier works of Oleg Losev with his published reports on light emission from zinc oxide and silicon

carbide crystal rectifier diodes in 1927 [8]. In the 1960s, the General Electric Company introduced the first commercially available LED devices based on inorganic compound semiconducting materials [6]. The development of organic EL devices was initially hampered by the high voltages--on the order of 100V or above--required to achieve major light output by injection of charge into organic crystals such as anthracene. However research in the field was stimulated by the findings of Tang and VanSlyke in 1987. In their work, the researchers from the Eastman Kodak Company demonstrated a novel thin-film device structure utilizing a two-layer architecture made from an aromatic diamine emissive layer and an organic small molecule carrier transport layer composed of 8-hydroxyquinoline aluminum (Alq_3). Their device was driven to significant brightness by a dc voltage as low as 2.5V [9].

The first account of EL from a semiconducting, conjugated polymer was reported in 1990 by Burroughes et al. and was based on an emitting layer of poly(p-phenylene vinylene) (PPV) [10]. Burroughes' OLED adopted the thin film layer device architecture which has become quite common for use in experiments (Figure 2-1). In this basic device architecture, indium tin oxide (ITO), which is sputtered onto a glass substrate, serves as the anode. In many cases, the polymer layers are spin coated over the ITO and a metal is thermally deposited over the polymers and serves as the cathode. The anode and cathode are then connected to an external circuit and forward biased with the positive voltage on the ITO anode. Additionally, each of the films thicknesses are between 10nm to a few hundred nanometers.

PPV was initially shown to emit in the green-yellow part of the spectrum, but several different polymer compositions of varying bandgaps have since exhibited

emissions with wavelengths scattered throughout the visible part of the spectrum [12, 13, 14]. Also, variations in device architecture such as multi-layered or stacked devices that incorporate enhanced carrier transport (or barrier) layers have been shown to increase light output efficiency and lower turn on voltages [15, 16]. More recently, at a meeting of the Materials Research society, it was reported that white OLEDs with an efficiency of 57 lumens per watt of power (lm/W), were produced in Japan [17]. Comparison of both conventional, inorganic and white-organic LEDs shows increase in efficiency over the years indicates the (Figure 2-2). It is noted that on average, fluorescent bulbs produce about 60-100 lm/W while incandescent bulbs produce 17 lm/W [18].

In this review of the literature, methods used to calculate hole mobility are presented along with some of the strengths and weaknesses of each method. First though, a brief summary of carrier recombination and light production in OLEDs, including a discussion of device physics, and device architecture is presented. A review of the electronic structure of conjugated polymers is also presented and provides a basis for the discussion of carrier transport in this special group of semiconducting, organic materials.

2.2.2 Organic/Polymer Semiconductor Physics

As their name suggests, some organic materials exhibit semiconducting behavior. The basis for this behavior is related closely to the formation of a double covalent bond between two carbon atoms. Double bond formation can be explained by the occurrence of specific bond angles as predicted by the valence-shell electron pair repulsion theory (VSEPR theory) as well as by the energies and locations of electrons as predicted by the Pauli Exclusion Principle and Molecular Orbital Theory. In the simple case of an ethylene molecule (Figure 2-3), the double bond that forms between carbon atoms requires that four electrons are shared between the two carbon nuclei.

Additionally, two of the electrons, one each from the carbons, are present in sp^2 hybridized orbitals (Figure 2-4) and overlap end to end to form a sigma bonding molecular orbital (σ-bonding MO) [19]. The two remaining electrons (again, one each from the carbon atoms) remain available for further bonding. However, as stated by the Pauli Exclusion Principle, these electrons cannot exist in the same quantum state (e.g., the same orbital or the same space and around the same nucleus) as the other two sp^2 electrons. Therefore, the remaining electron exists in unhybridized p-orbitals.

In each p-orbital, two regions of high charge density are located on opposite ends of the central nucleus and in the case of the preceding double bond, are positioned perpendicular to the σ-bond. For the second bond to form, the p-orbitals from each carbon overlap which results in formation of the pi-bond (π-bond) [20]. Constructive interference during the p-orbital overlap creates a π-bonding molecular orbital (MO), while that resulting from destructive interference is the π*-antibonding MO. Each essentially forms half of the total π-bond (Fig. 2-5).

As the backbone of organic molecules becomes longer, such as those consisting of four or more carbons, they can sometimes form conjugated systems of alternating single and double bonds. Conjugated systems may consist of a benzene ring, or a system of a few (<100) linked unit molecules (-mers) called oligomers, or longer chains (~1000-10,000) of –mers called polymers. The electrons associated with each carbon atom in these systems first fill the available orbitals (i.e., the closest to the atom outward to the valence π-orbitals), with the last pair of electrons occupying what is known as the highest occupied molecular orbital (HOMO). The next molecular orbital beyond the HOMO is known as the lowest unoccupied molecular orbital (LUMO). Interestingly, the π-bonds

that form the HOMOs and LUMOs of each carbon can actually overlap above the single bonds and in effect, the electrons in the double bonds are delocalized over the whole macromolecule [21]. The delocalized electrons that are weakly bound (known as the π-electron cloud) can be ionized relatively easily and the electron vacancy (hole) or surplus electron can travel along the molecule with relative ease [22]. The HOMO and LUMO therefore act similarly to the valence and conducting bands found in inorganic semiconductors with a band gap separating the two energy levels.

Polymers of various chain lengths result in varying band gaps. This is easily predicted by a simple substitution of a single system of repeat units combined to a chain of length 'L', into the free electron orbital model [23].

Consider the solution to the time-independent Schrödinger's equation for a free electron in a one dimensional potential well of infinite depth and width L as given by Equation 2-1 [24].

$$\Psi_n(x) = A_n \sin k_n x + B_n \cos k_n x \qquad (2\text{-}1)$$

The wave function in this well known "particle in a box" model are required to be continuous at the boundaries (i.e., x=0 at the origin and x=L at the width of the potential well), therefore the solution requires that for $\Psi_n = 0$ at point x = 0, and B_n must also be zero. Furthermore, for $\Psi_n = 0$ at x = L, the $\sin(k_n L)$ value must also equal zero. Therefore, the proper solution is summarized with Equation 2-2,

$$\Psi_n(x) = A_n \sin k_n x = A_n \sin \frac{n\pi x}{L} \quad (n = 1, 2, 3, \ldots) \qquad (2\text{-}2)$$

From this solution, it can easily be seen that,

$$k_n = \frac{n\pi}{L} \qquad (n = 1, 2, 3, \ldots) \qquad (2\text{-}3)$$

where k_n, known as the k-value has been related to a set of energy levels (energy eigen values, E_n) defined as

$$k_n = \sqrt{\frac{2mE_n}{\hbar^2}} \qquad (2\text{-}4)$$

In effect, the boundaries of the potential well have defined a discrete set of allowed k-values and therefore, a discrete set of energy eigen values as given in Equation 2-5

$$E_n = \frac{\hbar^2 k_n^2}{2m} = \frac{n^2 h^2}{8mL^2} \quad (\text{n} = 1, 2, 3, \ldots) \qquad (2\text{-}5)$$

where h is Planck's constant, m is the electron mass and n defines the energy level, i.e., is a set of quantum numbers [21, 23, 24, 25].

For a polymer of length L made up of N repeat units and separated by a distance d (i.e, L in Equation 2-5 approaches 'Nd' for long chains), we see that the energy values given by Equation 2-5 can be modified as given by Equation 2-6:

$$E_n = \frac{n^2 h^2}{8m(Nd)^2} \quad (\text{n} = 1, 2, 3, \ldots). \qquad (2\text{-}6)$$

The energies of the HOMO and LUMO levels of the chain are assumed to be defined by the π electrons from the N p-orbitals. Recalling that each molecular orbital is filled by two electrons, and that each orbital is separated by one energy level, the HOMO has the energy given by Equation 2-7 and that of the LUMO is given by Equation 2-8

$$E_{(HOMO)} = \frac{\left(\frac{N}{2}\right)^2 h^2}{8m(Nd)^2} \qquad (2\text{-}7)$$

$$E_{(LUMO)} = \frac{\left(\frac{N}{2}+1\right)^2 h^2}{8m(Nd)^2} \qquad (2\text{-}8)$$

Now, given that the energy necessary to promote an electron from the HOMO to the LUMO is called the band gap, or E_g, this value is easily defined as the difference between E_{LUMO} and E_{HOMO} as:

$$Eg = \Delta E = E_{LUMO} - E_{HOMO} = \left(\frac{\left(\frac{N}{2}+1\right)^2 h^2}{8m(Nd)^2} \right) - \left(\frac{\left(\frac{N}{2}\right)^2 h^2}{8m(Nd)^2} \right) = \frac{(N+1)\, h^2}{8m(Nd)^2} \qquad (2\text{-}9)$$

The limit, reached by large chains (large N), is given in Equation 2-10.

$$E_g = \frac{h^2}{(8md^2)N} \qquad (2\text{-}10)$$

From Equation 2-10, it can be seen that as the chain length increases (i.e., as N increases), the band-gap (E_g) decreases. However, because the electron density given by the alternating double bonds in conjugated polymer systems is not equally distributed, the inter-carbon lengths (the spacing between the carbon-carbon double bounds versus carbon-carbon single bonds) are not equal. Experimentally it has been shown that this result forces a limit below which the band gap of a given conjugated system will not decrease, even with added length of additional mer-repeat-units [26, 27]. The length at which no change in band-gap is attained is known as the saturation length.

There have been several successful attempts to engineer the conjugation lengths of the active conjugated systems for use in OLEDs thereby altering the band gap and hence, precisely tuning the emission wavelength of the devices [28, 29]. One of the notable challenges in tuning a material for a particular low band gap by increasing the chain length has been to achieve conjugation lengths that gives both the desired band gap and polymer solubility [28]. As was stated previously, one of the advantages of polymer OLEDs is in the fact that they are easily processible from solution.

2.2.3 Device Operation

The fundamental purpose of electroluminescent polymer devices is to convert electrical power into light. The processes involved in the production of light within an OLED are summarized simplistically in Fig. 2-6.

First, charges of opposite sign (i.e., positive holes and negative electrons) are injected from opposing electrodes by application of an external voltage (forward bias). The carriers then travel through additional layers which either promote or inhibit their motion. Finally, when the carriers of opposite sign travel close enough to attract one another, either in a special recombination layer or at the interface between the hole and electron transport layers, they recombine forming a singlet exciton which can then decay radiatively and results in emission of a photon [11].

One of the indicators used to describe how efficiently a device produces light is the external quantum efficiency, η_{ext}, which is the ratio of the number of photons emitted by the device (into the viewing direction) to the number of electrons injected. The reason viewing direction is important in this definition is because many of the photons that are produced emerge from the sides of the device or can be re-absorbed within the various organic layers. Therefore, η_{ext} is several times lower than internal quantum efficiency, η_{in}, which incorporates all photons produced over all angles and with negligible reabsorption [31].

Though the above summary of OLED device physics is presented in a very general form, it can be seen that one of the greatest challenges in this field is to increase the percentage of electron and hole pairs (excitons) that recombine radiatively at an interface or within an emitting layer in order to increase the quantum efficiency. To meet this challenge, one must control the number of carriers entering the various layers of the

device and also exploit the rate at which the carriers are able to move through each layer. Knowledge of parameters such as the band gap as well as the carrier mobilities becomes important to properly tune the location and rate at which recombination occurs and thereby increases the quantum efficiency [32].

To gain an appreciation of the device physics as it relates to the generic device architecture mentioned above, one must study the energy diagram of an OLED. A typical structure and band diagram (Figure 2-7). In the figure, EA is the electron affinity, IP is the ionization potential, HTL is the hole transport layer, LUMO is the lowest unoccupied molecular orbital, HOMO is the highest occupied molecular orbital, EML is the emitting layer, φ_a is the anode work function, φ_c is the cathode work function and E_v is the vacuum potential [33]. The LUMO and EA are equivalent to the conduction band in inorganic semiconductors and will therefore be referred to simply as the LUMO in reference to organic semiconductors. Additionally, the HOMO and IP are equivalent to the valence band and will all be referred to as the HOMO.

When a voltage is applied to the electrodes, such that the anode is biased positively, the electronic bands are bent in a manner similar to Figure 2-8. Ideally, this bending narrows the otherwise high energy barriers (φ_b) that are present at the electrode/polymer interface. Hence, hole injection from the anode Fermi level, E_{Fa}, and electron injection from the cathode Fermi level, E_{Fc}, are promoted to the organic layer's HOMO and LUMO, respectively. This injection is represented by the curved arrows which indicate carriers tunneling through the energy barrier, φ_b. Furthermore, the use of a high work function anode φ_a, such as indium-tin-oxide (ITO), and a low work function cathode φ_c, such as calcium, helps ensure that carrier current is not injection limited (i.e., the φ_b's are

low enough so that the rate of charge carrier injection is large enough to not limit the amount of current being conducted).

If the bias is instead applied with the opposite polarity (reverse bias), carriers are not able to surmount the potential barrier that is present at either of the electrode/polymer interfaces. In this case, with a negative potential placed on ITO (which has a large work function value) for example, the electrons would need to be injected into the polymer from ITO instead of Ca. This would result in the electrons being blocked from injection into the LUMO of the polymer due to the large φ_b. This phenomenon is commonly referred to as rectifying behavior and is characteristic of diodes [35].

In some cases it may be useful to reduce the number of carriers in a device. To measure a transport property of one particular type of carrier in a semiconducting polymer, for example mobility, the number of charges of the other carrier type being injected into the material must be limited. In other words, to make a "single carrier device", one must lower the carrier injection efficiency of a particular contact by selecting appropriate materials for the anode or cathode.

For example, to measure hole mobility in regioregular poly(3-hexyl-thiophene) (or RR-P3HT) diodes, a group led by Michael McGehee at Stanford University constructed "hole-only" devices. The devices employed aluminum cathodes with a work function of φ_c=4.2eV to have large mismatched energies with the LUMO of RR-P3HT at 5eV [36]. With this configuration, the electron injection energy barrier φ_b is equal to 0.8eV and therefore negligible electron injection.

In another example (Figure. 2-9), four materials and their respective work functions are shown as cathodes in a three layer device with MEH-PPV selected as the

semiconducting polymer (LUMO =2.8eV, HOMO = 4.9eV). Indium, with a work function of about 4.2eV offers the lowest electron injection energy barrier of φ_b = 1.4eV while gold, with a work function of about 5.2eV, offers the largest barrier with φ_b =2.4eV.

Comparing the various cathodes introduced in Figure. 2-9 with the resulting I-V curves of Figure 2-10, one can see that although the energy barriers for electron injection may vary between 1.4eV and 2.4eV, the overall current in the device remains the about same at a given voltage, indicating that electron injection from the cathode is not controlling current in the device.

These data are evidence that the device current is dominated by holes. In fact, holes are often cited as the major charge carrier in OLEDs because hole-mobility is generally higher than that of electrons in conjugated polymer materials [38].

Alternatively, an electron-only device can be assembled by mismatching the band-offset between an anode's work function, φ_a, and the organic semiconductor's HOMO, while maintaining a low barrier between the cathode and LUMO.

2.3 Charge Carrier Transport

2.3.1 Mobility

Charge carrier mobility (μ) is an important parameter to characterize the carrier transport and resulting performance of polymers that are used as electroluminescent materials in light emitting devices [39]. At low electric fields, the drift velocity (ν) is proportional to the electric field strength (E), and the carrier mobility is the proportionality constant between these two values [40]. Therefore, carrier mobility is defined as the carrier drift velocity per unit applied electric field:

$$\mu = \frac{\nu}{E} \quad \left(\frac{cm^2}{V \cdot s}\right) \qquad (2\text{-}10)$$

Polymer semiconductors are known to have low charge carrier mobilities in comparison to carrier mobility in inorganic materials. For example, the hole mobilities of a wide range of organic semiconductors for use in optoelectronic applications have been reported in the range of 10^{-7} to 10 cm^2/V-s while that of p-type gallium nitride, which is used in inorganic LEDs, has been reported at 400 cm^2/V-s [41, 42]. The low values for polymers are attributed mainly to disorder of the polymer chains in conjunction with trapping due to the presence of impurities [43, 44]. Extrinsic variables such as temperature and applied electric field strength are also known to affect mobility [45].

High carrier mobility results in faster response as well as to reduction of operating voltage in LEDs [44]. However, in a stacked structure a low mobility in one layer followed by a high mobility in the next layer can cause charges to accumulate and effectively form a parallel plate capacitor [46]. Knowing the mobilities of charge in the various layers can assist in designing an optimized device where charge is accumulated at the desired location(s).

Other conducting organic devices that depend on carrier mobility include organic field-effect transistors (OFETs). OFETs may be integrated into a number of products ranging from RFID tags to active-matrix displays. Similarly, a disadvantage of FETs that contain organic materials is that the active layer charge mobility, as compared to their inorganic equivalents, is relatively low [47]. However, OFETs may be processed with greater ease and have superior mechanical (flexural) properties. These advantages generally result in lower cost and a broader range of applications.

It is important to note the relationship between mobility and conductivity of a material. For the case of *n* free charge carriers per unit volume, each with a charge *q,* the charge density is *nq*. With the electric current density (J) defined as the charge density times drift velocity we have:

$$J = nq\nu \, . \qquad (2\text{-}11)$$

From Ohm's Law, the current density is defined as conductivity, σ, times the electric field:

$$J = \sigma E \qquad (2\text{-}12)$$

Equating Equations 2-11 and 2-12 results in:

$$\sigma E = nq\nu \, . \qquad (2.13)$$

Now, substituting for electric-field from Equation 2-10 above:

$$\sigma = nq\mu \qquad (2.14)$$

i.e., conductivity can be expressed in terms of the mobility [25]. It is important to note that a large drift mobility does not automatically equate to a high conductivity because σ also depends on the concentration of charge carriers.

Over the years, several experimental methods have been used to measure the mobility of charge carriers in semiconductors [36, 40, 41, 48, 49, 50]. Generally, these methods vary based on the way external fields affect charge carrier transport. For example, Hall mobilities rely on the effects on charge carriers of both electric and magnetic fields. The time-of-flight method relies on a pulsed external light source, such as a laser, to generate carriers in combination with an applied electric field. Finally, the space charge limited current method (SCL or SCLC) relies solely on an applied electric-field to inject and transport the carriers [48]. Each of these methods is discussed below.

2.3.2 Hall Effect Method

An electric field (E_x) applied to the x-axis of a sample along with a magnetic field (B_z) applied perpendicularly along the z-axis, gives rise to a traverse electric field (in the y-direction) which exerts force on the charge carriers. As carriers are forced in the y-direction, the induced electric field E_y (the Hall field), which is derived from the induced potential (V_y) and thickness of the sample in that direction (W), balances the force induced by the magnetic field [40]. From the Hall Effect, it can be shown that:

$$E_y = \left(\frac{V_y}{W}\right) = R_H J_x B_z \ , \qquad (2\text{-}15)$$

where R is the Hall coefficient and is equal to (1/nq) and J_x is the current density of the charges flowing in response to E_x. R_H can be determined from the values of E_y, J_x and B_z using Equation 2-15. If one type of carrier dominates, the carrier concentration and type can be determined from the Hall coefficient. The carrier mobility can be determined using Equation 2-16 [25].

$$R_H \sigma = \mu \ . \qquad (2.16)$$

In 1958, a method was developed that exploits the Hall Effect, but is modified for measurement of flat samples of arbitrary shape [51]. This method, known as the Van der Pauw technique, has been commonly used for measuring transport properties of many inorganic semiconductors such as p-GaN, n-InN and n-InGaN having mobilities of 46, 2 and 107 $cm^2V^{-1}s^{-1}$, respectively [52]. However, the Van der Pauw technique is not commonly used to measure the carrier mobility of polymers. Though organic samples can be prepared to meet the requirements for applying this technique, the current density, J_x, is often too low to induce a measureable Hall voltage. Essentially, the carrier mobility in conjugated polymers is usually too low to be measured by the Hall Effect [53]. The

Hall voltage, which is typically in the range of a few meV even for high mobility materials, is too low in polymers, resulting in a signal-to-noise ratio that is very low.

Mobilities in polymers have been reported utilizing the Van der Pauw technique/Hall Effect. For example, the Hall mobility of AsF doped (17%) polyacetylene was reported to be ~$2x10^{-2}$ $cm^2V^{-1}s^{-1}$ [54]. In another case, the Hall technique was used to measure mobility in poly(4,4-dipentoxy-2,2'bithiophene). Results were comparable to amorphous inorganic semiconductors with values of 10^{-1} to 10^2 $cm^2V^{-1}s^{-1}$ [43].

2.3.3 Time of Flight

The time-of-flight technique is the most widely used method to measure mobilities in organic conductors [49]. In this method, the organic material is placed between two electrodes, one of which is transparent and does not inject carriers. A sheet of charge carriers is photogenerated by external pulsed laser or lamp illumination through the transparent electrode and the carriers move through the sandwiched sample to the other electrode under the influence of an applied electric field [55].

To determine the hole mobility, a thin charge layer may be generated near the anode (Figure 2-12. In this case, the light pulses must not be absorbed in the cathode or by the sample. Photogeneration must take place at the generation layer and electrons collected at the nearby anode, while holes migrate across the complete thickness of the sample layer [56].

A transient photocurrent profile is recorded and a clear inflection point is determined from the current-decay pattern [57]. The inflection point, is the intersection of two tangents on the log current-log time plot (Figure 2-13), and is equal to the carrier

transient time, T_{tr}, of the fastest carriers [44]. In other words, T_{tr} is the time required for the photogenerated carriers to reach the opposite transparent electrode.

The charge carrier mobilities are then calculated by manipulating Equation 2-11 into:

$$\mu = \left(\frac{d^2}{T_{tr} \cdot V} \right) \qquad (2\text{-}17)$$

where d is the sample thickness and V is the applied bias.

Utilizing the time of flight method, Kaneto et al. has reported hole mobility of regioregular poly(3-hexylthiophene) (MW 29 kg/mol) of $\mu_h = 4x10^{-4}$ $cm^2/V\text{-}s$ for drop cast films having a thickness of 7μm [41].

TOF requires thick films so that the absorption depth of the optical excitation is small compared to the sample film thickness. TOF experiments on poly-phenylene-vinylene (PPV) for example, have been reported with film thickness of 1-10μm. To attain such thickness, the deposition by spin-coating requires slow spin rates. Therefore it is preferable to form thick films by drop-casting. Unfortunately, preparation by this method can influence mobility because the material structure of drop-cast films differs from that of spin-cast films [45]. Differences in mobility measured by TOF between drop cast and spin coated films have been reported for regiorandom-poly(3-hexylthiophene). These mobilities were $\mu = 10^{-7}$ $cm^2/V\text{-}s$ for drop cast films having a thickness of 5400nm, and $\mu = 10^{-5} cm^2/V\text{-}s$ for the spin deposited films having thickness of 200nm [41].

Determining the TOF-mobility of films with a distribution of mobilities (dispersive transport) is also complicated since the arrival of carriers at the electrodes is spread out

and usually the fastest carriers make up the bulk of the measurement [53].

2.3.4 Space Charge Limited Current

Charge transport through a thin organic polymer film is said to be either an electrode limited process or a bulk limited process [39]. In an electrode limited process, carrier injection is "limited" by the energy barrier between the electrode's work function and the polymer's HOMO or LUMO levels, depending on whether the injected carrier is a hole or an electron, respectively. In a bulk limited process, carrier transport is limited by the drift velocity through the material, i.e., the mobility of the charge carrier.

When the relationship between current (I) and voltage (V) is linear, it is indicative of an ohmic system. This is the case for transport in metals where the I-V relationship is described by Ohms' law, V = IR, or alternatively with respect to current density (J),

$$J = q\mu n\frac{V}{d}. \qquad (2\text{-}18)$$

In this modified version of Ohm's law, q is the carrier's charge, n the charge carrier density, μ the carrier mobility, V the applied voltage, and d the thickness of the sample. This is also typically the case at low voltages when injecting carriers from a metal contact into a conjugated semiconducting polymer. However, a point exists where this condition breaks down and non-linear I-V behavior, characteristic of all organic LEDs and known as space charge limited current (SCLC), is observed [58]. At higher voltages, more carriers are being injected across the barrier, and at a faster rate than they can travel through the polymer and exit at the other contact. This results in charge accumulation near the injecting electrode which redistributes the electric field intensity, controls transport through the polymer bulk and determines the I-V dependence [59]. In practice,

when at least one of the interfacial barriers is lower than ~0.3eV, the current in an organic LED will be SCLC [60].

In cases where these conditions apply plus no traps are present in the polymer film and the mobility is independent of the field, Equation 2-19 describes trap free space charge limited current.

$$J = \frac{9}{8}\varepsilon_o \varepsilon_r \mu \frac{V^2}{d^3} \qquad (2\text{-}19)$$

where ε_o and ε_r are the permittivity of free space and relative permittivity, respectively [61, 62]. Conversely, due to their intrinsically disordered nature, the carrier mobility in most conjugated polymers is field dependent [36, 63]. Equation 2-19 has therefore been modified as

$$J = \frac{9}{8}\varepsilon_o \varepsilon_r \mu_0 e^{.89\gamma\sqrt{E}} \frac{V^2}{d^3} \qquad (2\text{-}20)$$

Utilizing either Equations 2-19 or 2-20, it is possible to extract the charge carrier mobility by fitting the experimental J-V data [39]. To prevent charge recombination, single carrier devices as previously described must be constructed. This allows for measurement of the current and resulting mobility for either electrons or holes. Unfortunately, since the work function of one of the electrodes has to be adjusted to make the device either a hole-only or electron-only diode, the electron and hole mobilities cannot be measured with the same device [53].

Hole mobility was measured for poly(3-hexylthiophene) in the space charge regime. It was found that the lower molecular weight samples had mobilities that were field-dependent. Fig. 2-14 shows a plot of $J^{0.5}$ vs V for low molecular weight poly(3-

hexylthiophene) and film thicknesses of 96nm and 192nm. The inset shows non-linear J vs V_{bias} characteristic, indicative of space charge limited current.

Equation 2-19, shown as the dark straight lines in Figure 2-14, does not fit the data well, especially for the 96nm sample. However the data overlaps the dashed line, which is Equation 2-20, reasonably well. This indicates that the hole mobility in fact is field-dependent in low MW samples of poly(3-hexylthiopene). The resulting hole mobilities varied from $1.33 \pm 0.41 \times 10^{-5}$ $cm^2/V\text{-}s$ (MW 2.89 kg/mol), $1.13 \pm 0.37 \times 10^{-4}$ $cm^2/V\text{-}s$ (MW 9.72 kg/mol) and $3.3 \pm 0.73 \times 10^{-5}$ $cm^2/V\text{-}s$ (MW 31.1 kg/mol) and are in agreement with the time of flight measurements of Kaneto et al. as reported above [36].

To date, several other I-V experiments have been performed on various polymers to determine carrier mobility from the space charge limited current model [39, 64, 65]. The present study will use this SCLC method to determine the hole mobilities of poly(3,4-propylenedioxythiophene-diethylhexyloxy)-cyano-p-phenylene-vinylene substituted with dodecyloxy chains on the phenylene ring.

2.3.4 Trap Charge Limited Current

For trap-free films, the space charge model predicts that $I \alpha V^2$. Yet in an early assessments of space charge in inorganic materials, Smith and Rose observed a high power dependence ($I \alpha V^m$ with $m > 2$) for insulating CdS crystals and attributed this to the filling of traps followed by an excess of charges after all the traps are filled, resulting in an increased number of carriers [66]. While they recognized that the presence of traps can determine the relationship between current and voltage (i.e., the power law dependence), they did not apply this model to organic materials. More recently, the presence of traps in anthracene has been reported with a very high power exponent of

$I \alpha V^{12}$ (at T = 20°C) [67].

Organic materials such as conjugated polymers may have traps present as a result of structural disorder, impurities, geminate pairs or self-trapping [68]. Traps affect the charge transport properties by removing carriers that contribute to the charge transport. When traps have a continuous exponential energy distribution, the dependence of current on voltage for this I-V region is called trapped-charge limited. It is in this region that as the applied forward bias is increased, traps below the quasi Fermi energy level for a specific carrier are filled. During the trap-filling the trap-free space charge equation (Equation 2-19) must be modified to reflect the fact that not all carriers are available for transport. The relation between J and V for trapped-charge-limited currents (TCLC) is defined by Equation 2-21:

$$J = N\mu q^{1-m}\left(\frac{2m+1}{m+1}\right)^{m+1}\left(\frac{\varepsilon m}{Nt(m+1)}\right)^{m}\frac{V^{m+1}}{d^{2m+1}} \qquad (2\text{-}21)$$

where N is the density of states in the conduction band or the valence band, Nt is the total trap density, m = Tc/T where Tc is the characteristic temperature of the traps, T the absolute temperature, and the balance of the terms are defined above. At high current, all the traps are filled and they no longer affect charge carrier transport. The current at this point behaves similar to that of a trap-free space-charge limited current [65].

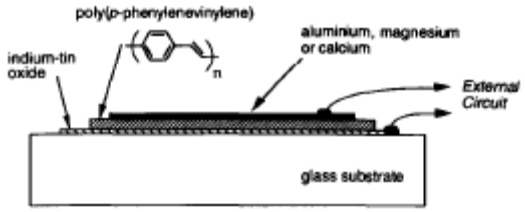

Figure 2-1. Structure of polymer LED (OLED) [11]

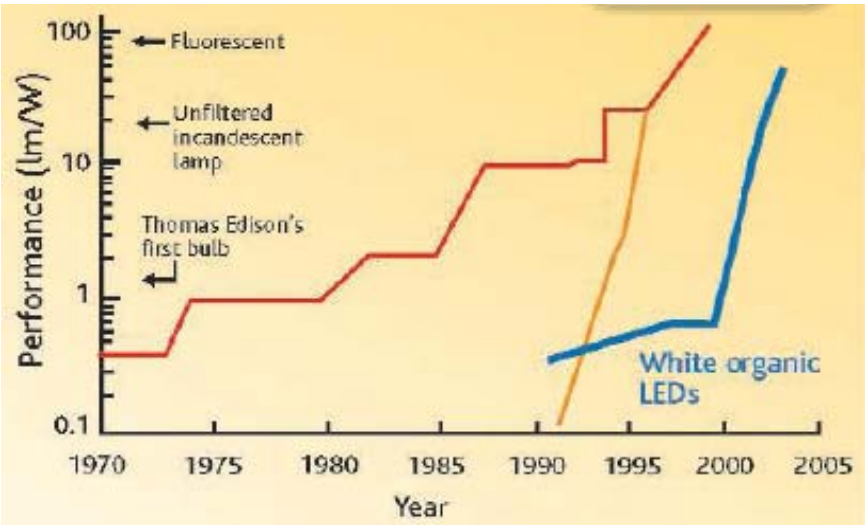

Figure 2-2. Progress in LED efficiency [17]. Red line is conventional LEDs.

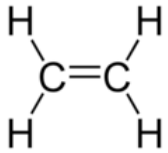

Figure 2-3. Ethylene molecule Lewis Structure

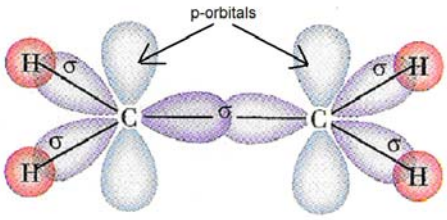

Figure 2-4. Ethylene molecule depicting s-oribitals, sigma bonds and p-orbitals [19].

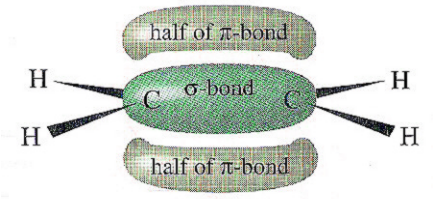

Figure. 2-5. Depiction π-bonds in ethylene molecule [20].

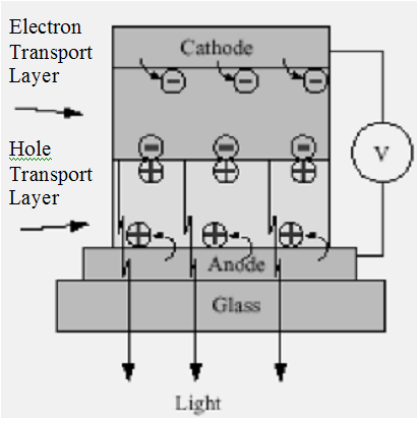

Figure 2-6. Summary of carrier transport and recombination in OLEDs [30].

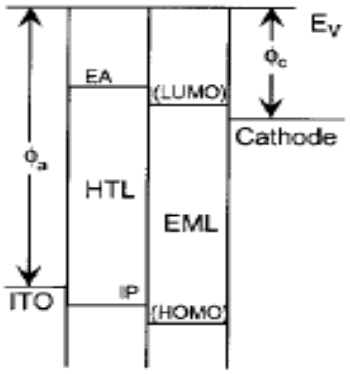

Figure 2-7. Energy band diagram of typical OLED [33].

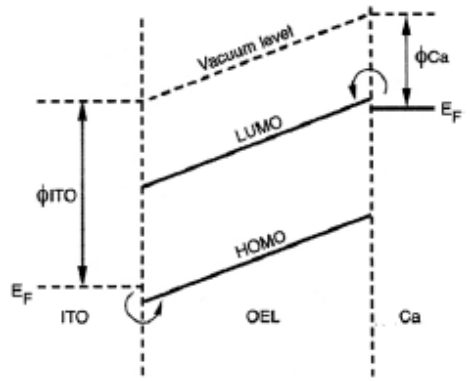

Figure 2-8. Band diagram of an organic electroluminescent layer (OEL) under forward bias [34].

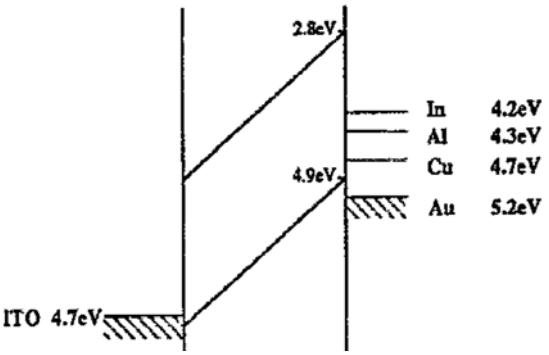

Figure 2-9. Three layer device depicting four possible cathode materials [37].

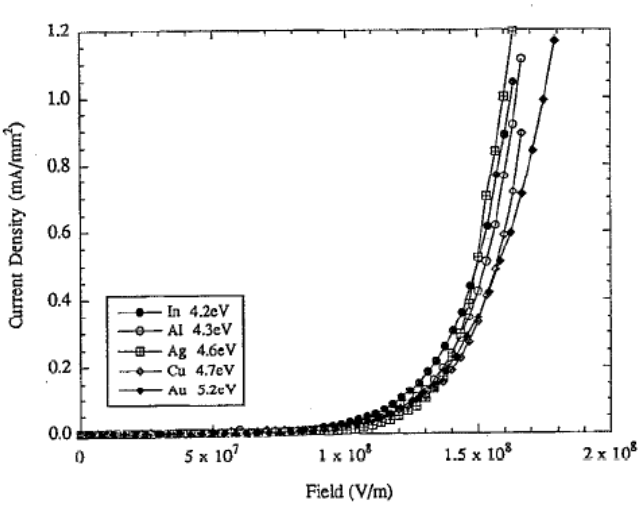

Fig. 2-10. I-V for ITO/MEH-PPV device with various anodes [37].

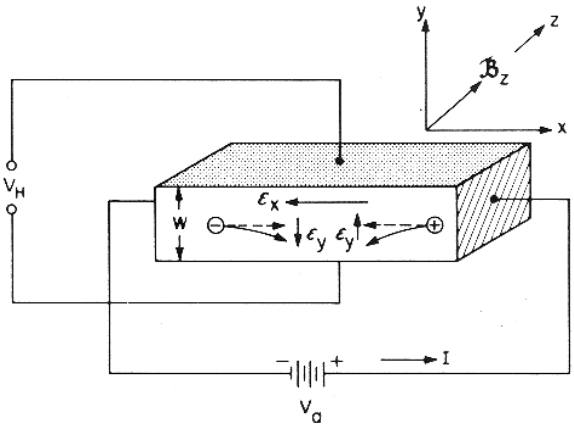

Figure 2-11. Basic setup to measure carrier concentration using the Hall effect [40].

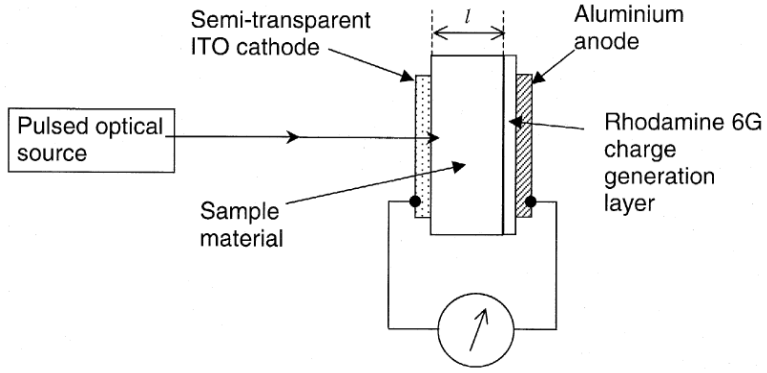

Fig. 2-12. Time of Flight Experimental Setup [56]

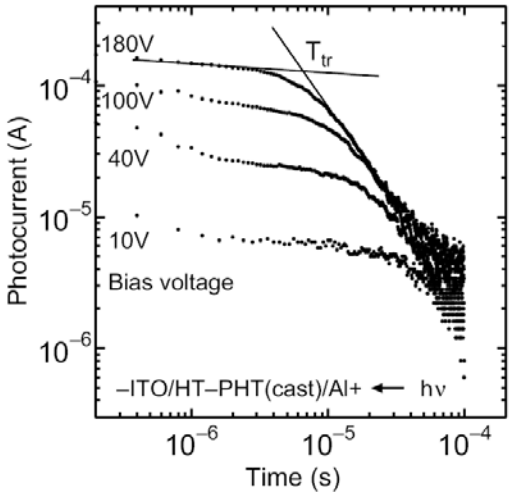

Fig. 2-13. Time of Flight photocurrent profile at various applied bias voltages [41].

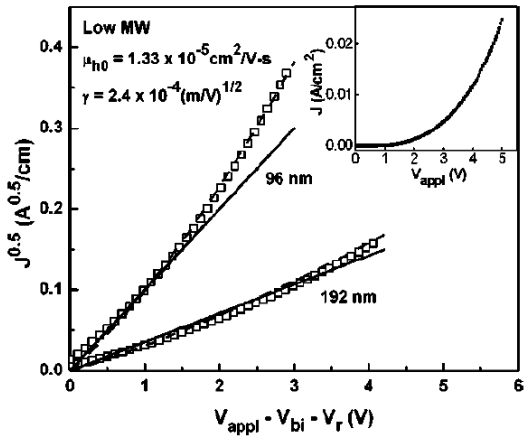

Figure 2-14. $J^{0.5}$ vs. V plot for low MW (29.9 kg/mol) poly(3-hexylthiophene).

CHAPTER 3
EXPERIMENTAL METHODS

3.1 Introduction

This chapter describes the various tools, techniques and procedures which were used to prepare samples and collect the experimental data reported and discussed in this thesis. First, the method used to prepare the indium tin oxide (ITO) coated glass substrates is described. The next section describes device architecture and how devices utilizing a high work function anode and cathode were used to ensure single carrier transport. The use of a simple two point probe setup to measure current (I) versus voltage (V) applied to the devices is then described. Next, the use of profilometry and atomic force microscopy (AFM) to characterize film structure is summarized. Last, an overview of the software utilized for data analysis and computation of carrier mobility (μ_h with units $cm^2/V \cdot s$) is presented.

3.2 Device Preparation

3.2.1 Substrate Cleaning and Etching

Glass slides coated with 150-200 nm films of ITO were purchased from Delta Technologies, Ltd.. The slides measured 1 x 1 inch-square were reported to have a sheet resistance (R_s) of 8-12 Ω per square CB40-IN Corning 1737 ITO One Surface). To begin the process of device fabrication, the ITO was patterned by a room temperature acid vapor etch. The acid used was a mixture of three parts hydrochloric acid (HCl) to 1 part nitric acid (HNO_3) by volume, commonly referred to as aqua-regia. This step makes it possible to later deposit metal contacts on the device in such a way as to make eight

devices on a single substrate. To remove the ITO in select areas, a mask made of simple scotch-tape was utilized to expose specific areas of the slide to the aqua-regia vapor for approximately 10 minutes. After etching, the areas were tested with an ohmmeter to verify that resistance was over 1 Mega-ohm, indicating that the ITO had been removed. Figure 3-1 summarizes this process and shows the ITO pattern remaining on the slide after the aqua-regia etch.

Because of the contamination that occurs when samples are handled, packaged, exposed to air, and then ITO etched, the samples were subsequently cleaned to remove dust, organic contaminants and adhesive residue from the scotch-tape mask. First the substrates were placed in a beaker filled with a "detergent" solution of 20mg of sodium dodecyl sulfate dissolved in 500mL of de-ionized water. The beaker was then placed in a sonicator and the substrates were cleaned for approximately 15 minutes. Next, the detergent solution was emptied and the beaker was then filled only with deionized water and the samples were again cleaned in the sonicator. This process was repeated three more times using solutions of methanol, acetone and finally, 2-isopropyl alcohol. Used solvents were distilled for reuse in this process. The cleaned substrates were placed in clean slide cases and then in vacuum sealed desiccators to limit exposure to moisture and environmental contaminants.

3.2.2 ITO Surface Treatment

After the samples had been cleaned and stored as described above, they were inserted into a HARRICK PDC-32G Plasma Cleaner and exposed to an oxygen plasma for 20 minutes just prior to polymer coating. During the oxygen-plasma treatment, the ITO undergoes physico-chemical and electronic property modifications, including a smoother surface, higher surface energy with high polarity, and an increased work

function [69]. A smooth and high-polarity ITO surface promotes better adhesion of a polymer film and reduces the interfacial tension between the polymer and substrate. The increased work function, which is attributed to removal of organic surface residues during oxygen ion bombardment, results in increased hole injection due to the decreased energy barrier between the conduction band of ITO and the HOMO level of the polymer [70].

3.2.3 Addition of Hole Transporting Layer

After the samples have been exposed to the oxygen plasma, the next step is to deposit the polymer layers. A hole transporting layer (HTL) consisting of Poly(3, 4-ethylenedioxythiophene)-poly(styrenesulfonate), otherwise known as PEDOT-PSS (Bayer Baytron P VP A1 4083), was spincast over the ITO plus the etched areas of the substrate (Figure 3-1). Subsequently, the active polymer film was also deposited by spin coating because of its ease and reliability in creating uniform thin films [4]. For spin casting, the samples were placed on the sample-holder of a Chemat Technology, Inc. model KW-4A spin coater. The spin coater spin rate was set manually with the revolutions per minute (RPM) displayed on an LCD. While the sample was at rest, 400μL of PEDOT-PSS in an as prepared aqueous solution (Bayer Baytron® P VP A1 4083) filtered through a 0.2μm nylon filter, was added using a micropipette. Once the PEDOT-PSS covered the entire surface of the sample, spinning was initiated at a rate of 3000 RPM. During the spin coating process, most of the polymer solution was removed from the substrate by centripetal force. After a short time (about 15 seconds), a thin liquid film is left on the surface and the solvent evaporates which results in an increase in the viscosity of the film [71] thereby resulting in the final film thicknesses of 40 nm. In

the present study, once the PEDOT:PSS was spin coated onto the substrate, the samples were placed in a vacuum oven and baked at 150^{o}C for 4 hours to completely remove all solvent (water) from the films. When the films were dry, the slides were placed in an argon atmosphere of an isolated glove box. For each run, which included preparation of several devices, one slide with only the PEDOT-PSS layer was set aside to be used as a reference in determining the layer thickness by profilometry.

3.2.4 Addition of Active Layer

Research has shown that device characteristics are strongly influenced by the presence of moisture [72]. Therefore, a glovebox (Figure 3-2) manufactured by MBraun GmbH and filled with dry argon was utilized to complete the device fabrication by adding the active layer and top cathode contact. .

Spin coating of the active polymer, gold contact deposition and current-voltage measurements are all performed within the glove box to prevent exposing the devices to moist air. Though the glove box ambient is pure argon (99.9% from Praxair), oxygen and water concentrations can increase when samples are transferred from the outside environment into the glove box. All experiments were performed with less than 5ppm oxygen and 5ppm water. Solutions ranging between 8 to 28 mg/mL of poly(3,4-propylenedioxythiophene-diethylhexyloxy)-cyano-p-phenylenevinylene substituted with dodecyloxy chains on the phenylene ring ("PProH") in di-chlorobenzene or toluene solvent were prepared in small glass vials. Similarly, 20 mg/mL solutions of poly(3-hexyl-thiophene) ("P3HT") in dichlorobenzene and of poly(3,4-propylenedioxythiophene) ("PProDOT") in toluene were prepared. Prior to being placed in the glove box, the polymer solutions were placed in a glove-box load-lock. In order to reduce the amount of oxygen and moisture from the contents entering the glove-box, the

load-lock is exposed to a double decontamination cycle where the load-lock contents are exposed to a vacuum of approximately 25 in. Hg , refilled with argon, exposed once again to the same vacuum, and finally equilibrated with the glove-box atmosphere.

A volume of 300μL of the active polymer solution was then added over the PEDOT-PSS layer in an even fashion using a micro-pipette. Spin rates ranging from 700rpm to 1200rpm were used to produce a range of PProH, P3HT and PProDOT film thicknesses. After spin coating the polymer layer over the PEDOT-PSS, the samples were prepared for metal top electrode deposition. Once again, devices were placed in a vacuum oven and baked at 150^{o}C for 4 hours to completely remove all solvent (toluene or dichlorobenzene) from the films.

3.2.5 Vapor Deposition of Gold Electrodes

A stainless steel shadow mask, patterned as in Table 3-2 to allow for eight different connected dot electrodes per 25 x 25 mm^2 slide, was placed against the polymer film. The slides were then placed in a vacuum thermal evaporator system which was pumped down to 10^{-6} Torr using a turbomolecular pump backed by a oil –sealed roughing pump. Three or four pieces of Au-shot ~1 mm in diameter were placed in a tungsten boat that was clamped between two post connected to electrical feed-throughs. Au evaporation was monitored by the MBraun integrated thin film deposition controller with a deposition rate for gold inputted at 2.5 Å/s. Deposition stopped automatically when the film thickness reached 100nm. After deposition, the samples were allowed to cool for 1.5 hours. The thermal evaporator was then backfilled to 1atm with argon from the glove box. Figure 3-3 summarizes the device fabrication including cathode deposition.

3.3 Current-Voltage Measurements

3.3.1 Keithley Source Meter

Current-Voltage (I-V) data were collected to determine the hole mobility (μ) in the active polymer layer using a two point probe technique to apply a bias voltage between the anode and cathode electrodes. Two probes, one which is biased positively and the other biased negatively during measurement, were attached to a Keithley Series 2400 source-meter. The voltage step and rate, starting voltage and end voltage were specified utilizing the LabTrace software package from Keithley. The positive probe was contacted to the ITO surface (exposed by rubbing as described below) and the negative probe contacted the vapor-deposited gold electrode.

3.3.2 Sample Holder

The custom sample holder (Figure 3-4) was used to hold each sample for I-V measurements. The holder has 12 pins that are static on one side and the Keithley probes are connected to these pins by alligator clips (Figure 3-2).

The other end of each pin fits through a hole in the holder and makes contact with the sample with spring loaded, gold contacts. Eight of the pins which are located around the center of the holder are designed to be compressed against the eight gold cathode electrodes of the sample (Figure 3-3, step #5). The remaining four pins located at the corners of the holder are compressed against the ITO (anode) surface of the samples, where the active polymer and PEDOT:PSS layers were removed by rubbing each corner with a cotton swab saturated in dichlorobenzene. In this process, single strokes were used to avoid redeposition of material on subsequent strokes. While the active polymer was removed by dissolution in the dichlorobenzene, the PEDOT-PSS was removed by mechanical force. Removal of the polymer layers was verified visually by a change in

the reflective properties of the corner areas versus the remainder of the sample which was still covered with polymer. For further verification of removal, the resistance between the pins contacting the ITO was measured. If the resistance between two pins was 100Ω +/-20Ω, then it was concluded that the pins were touching the ITO. If resistance was much higher than this value, the sample was removed from the holder and another swab with solvent was used to remove the polymer layers. This process was repeated until the resistance between all pins contacting the exposed ITO surface was sufficiently low.

3.4 Structural Characterization

3.4.1 Profilometry

To measure the thickness of the active conjugated polymer layer, a cotton swab was used, as described above, to remove the active polymer and PEDOT-PSS layers again to expose the ITO. In this case, material was removed along narrow paths running parallel to two edges of the samples, from one end to the other. Visual inspection was used to verify that the polymer layers had been removed. Each path where the polymer was removed consisted of a trough surrounded by layers of polymer. A Tencor Alphastep 200 surface profilometer was used to measure the depth of the troughs and therefore the total thickness (d_{tot}) of both polymer layers. The same material removal procedure was used to produce troughs on the samples with only a PEDOT-PSS layer, one of which was prepared for each batch of samples as reported above. The thickness of the PEDOT-PSS layer (d_{PEDOT}) was also measured using the profilometer. The difference between d_{tot} and d_{PEDOT} is then equal to that of the active polymer (d_p).

3.4.2 Atomic Force Microscopy

Atomic force microscopy (AFM) images were taken with a VEECO Dimension 3100 AFM at the University of Florida in the Major Analytical Instrumentation Center

(MAIC). The same samples that were prepared for measurement with the profilometer were also measured in the AFM for comparison. Images were taken in the tapping mode and the thickness of the polymer layers was determined. The root-mean-square surface roughness (RMS roughness) was also determined.

3.5 Experimental Procedures

3.5.1 Film Thickness Variation

By varying the rate at which films were spin-deposited between 700 to 1000 revolutions per minute, the thickness of the active conjugated polymer films were varied. Other parameters such as ITO surface-treatment time, spin speed of the PEDOT-PSS layer, and volume of polymer initially added to the substrate were kept constant. The hole mobility was measured as a function of the active film thickness.

3.5.2 Increased Temperature Exposure

Current-Voltage data were collected from as prepared samples. The samples were then placed on a hot plate, while still inside of the glove-box, and heated in argon to approximately 100^{o}C for 4 hours. The temperature of the hot place surface was verified with a thermocouple. I-V data was again collected for the samples after they were allowed to cool for 30 minutes.

	Step	Top View	Side View
1.	A clean 25 x 25 mm square of ITO on a glass substrate is used for etching.	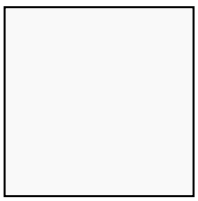	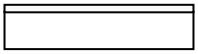
2.	ITO is etched. The light areas indicate area where ITO was removed using aqua-regia acid vapor.	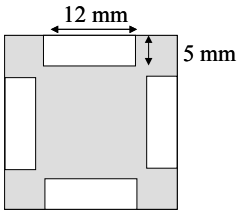	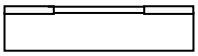

Figure 3-1. Summary of ITO patterning procedure.

Figure 3-2. Braun Glove Box used for sample preparation.

	Step	Top View	Side View
3.	PEDOT-PSS is spin coated onto the etched ITO surface and then baked and vacuum dried.	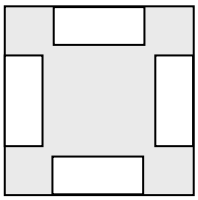	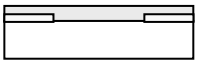
4.	The active polymer is spin coated on top of the PEDOT:PSS layer in the dry box.	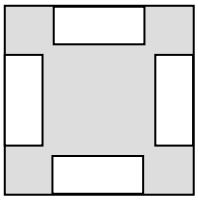	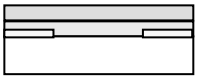
5.	The metal electrodes are vapor deposited on top of active polymer in the dry box.	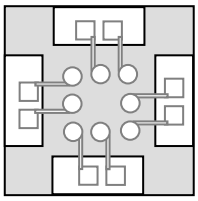	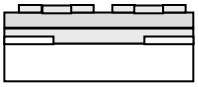

Figure 3-3. Continuation of device preparation, showing (3) PEDOT-PSS hole transport layer, (4) PProH active polymer layer, and (5) Au metal contact depositions.

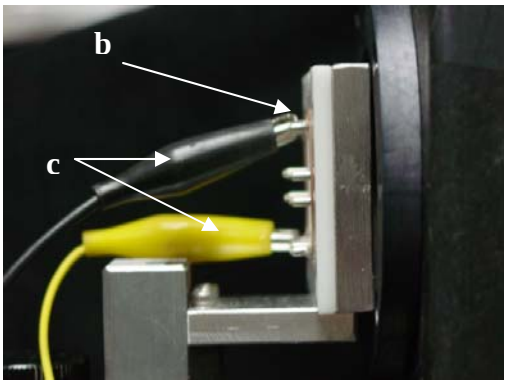

Figure 3-4. Sample Holder (a) with pins (b) and measurement probes (c) attached.

CHAPTER 4
EXPERIMENTAL RESULTS

4.1 Background

In this experiment, current-voltage (I-V) data were collected and compared with the space-charge limited current model (as presented in section 2.20) to extract the hole mobility of the conjugated polymers. Current-voltage (I-V) data are taken for devices with active polymer layers of poly(3,4-propylenedioxythiophene-diethylhexyloxy)-cyano-p-phenylenevinylene substituted with dodecyloxy chains on the phenylene ring ("PProH"), poly(3-hexyl-thiophene) ("P3HT"), or poly(3,4-propylenedioxythiophene) ("PProDOT") films (Table 4-1 for the chemical structure of these materials). To extract hole mobilities from I-V data, three values are required: applied voltage (V_{bias}), the resulting current density (J), and the polymer film thickness (d). Although current and voltage are collected with an automated Keithley controller, control and measurement of the film thicknesses provided the biggest challenge in the experiment. Even after the rigorous cleaning steps discussed in Chapter 3, deposition of smooth and uniform polymer films was hindered by particulates on the sample surfaces or the effects of different solvents during spin coating. For example, inconsistent surface wetting by the various polymer solutions on the glass/ITO/PEDOT-PSS samples sometimes resulted in non-uniform active layer thicknesses on the samples. This will be discussed further as the experimental results, such as surface characteristics of the various deposited polymer films and the calculated hole mobility, are reported below.

4.2 Results

4.2.1 Physical Characterization

4.2.1.1 Film preparation for thickness measurements

Polymer films were spin coated onto a glass substrate coated with a transparent conducting indium tin oxide (ITO) and a PEDOT-PSS layer. Film thicknesses for a given solution were varied by changing spin rates between about 700 to 1000 rpm for a constant 30 seconds. To prepare the samples for thickness measurements, portions of the films were removed by scratching straight lines across the samples with a sharp edge. This process removed polymer from the surface of the glass/ITO substrate making small channels down to the surface of the ITO. As depicted in Figure 4.1, control samples on which only PEDOT-PSS was deposited over ozone plasma treated ITO-on-glass substrates were measured. Once other films were deposited over the PEDOT-PSS, it becomes difficult to measure the PEDOT-PSS thickness so samples with only PEDOT-PSS were first measured to determine its film thickness. The dark horizontal lines in Figures 4-1 and 4-2 represent the channels formed by scratching the films with the edge of a razor blade, and the channels are represented as breaks in the upper film layer.

With only PEDOT-PSS deposited on the glass/ITO substrate, measurement across the channels with the AFM tip provided the thickness of the PEDOT-PSS layer (i.e., d_{DOT}). Because the spin rates and spin times were held constant for PEDOT-PSS deposition, it was assumed that the thickness of the PEDOT-PSS films for all samples was constant. Approximately 300mL of an as-received aqueous solution of PEDOT-PSS (Bayer Baytron P VP a1 4083) [73] was filtered using a .2μm filter and then spun at 3500 rpm for 30 seconds resulting in films with 40 ±10 nm thickness.

After determining the PEDOT-PSS thickness and as depicted in Fig. 4.2, scratches were also formed across samples having both PEDOT-PSS as well as additional active polymer films.

The channels on these samples provided a "depth" over which to measure the total thickness (i.e., d_{TOT}) of all films deposited over the ITO. By substracting the known PEDOT film thickness from the total thickness of all films measured by AFM, the polymer film thickness (d) was determined by simple calculation utilizing Equation 4-1.

$$d_{TOT} - d_{DOT} = d \qquad (4\text{-}1)$$

The above method determined the film thickness used in the space charge and trapped charge limited current models. However it is based on the two assumptions that the PEDOT-PSS thickness was constant across all samples, and that none of the ITO film was removed by scratching.

4.2.1.2 Atomic force microscopy

Polymer film thicknesses were first measured by profilometry, however there were small scratches on the samples after this procedure, raising concerns that the metal tip of the profilometer caused damage to the delicate polymer surface. Therefore, AFM was adopted as the appropriate measuring technique for this experiment. The AFM allowed for better thickness measurement precision, as well as a better and more quantitative understanding of film topography by visual representation of the surfaces and quantification of the root mean square (RMS) surface roughness.

AFM measurements were taken only after the I-V measurements were completed. In order to measure the film surface, the samples were removed from the inert gas glove box and thereby exposed to laboratory air. Once exposed to air and humidity, no further electrical measurements were collected. Although no further electrical measurements

were made after samples were removed from the glove box, samples were nonetheless stored in clean, single-slide plastic containers. The containers were further stored in desiccators and kept under vacuum. This storage technique was used as a precaution to minimize surface contamination during physical transport of the samples between labs and testing areas.

To characterize the film surfaces, the 1x1 cm samples were cleaved into smaller ~5x5 mm sections so as to fit properly in the AFM sample holder. For these measurements, cleaved samples were inspected by eye and selected based on proximity of the cleaved portion to the gold cathode areas. By selecting these proximity areas, it was assumed that measurements were representative of the film surface directly below the gold contacts where the carrier transport of interest occurs during I-V measurements. The result of a typical roughness analysis based on the AFM data with the RMS surface roughness of the area is highlighted (Figure 4-3).

To determine the thickness, the AFM was operated in the section analysis mode. Various points along the scratched channels were measured by the AFM to determine the thickness. Fig. 4-4 shows a typical analysis of the total film thickness (i.e., d_{TOT}).

In Figure 4-4, the vertical distance between two points located at the bottom of a channel (e.g., the left side red-arrow in the figures) and the surface of the polymer film at a location near the channel (e.g., right side red-arrow in the figures) was measured as 62nm (i.e., d_{TOT} = 62nm). It must be noted however, that because the film surface varied, appearing as a series of non-uniform peaks and troughs on the AFM output, the film thickness measurement is based on the assumption that the two points chosen were representative of average film thickness. By utilizing the above thickness Equation and

subtracting the thickness for PEDOT of 40nm, the polymer film thickness for this particular sample was easily calculated as: 62nm-40nm = 22nm.

Table 4.2 summarizes the film thickness and RMS surface roughness values for all films used in this experiment. Also included in the table are the solvents in which the polymers were dissolved, the concentrations of solutions based on weight of polymer to the volume of solvent, and the spin rates used to deposit each of the films.

4.2.2 Electrical Characterization

4.2.2.1 Current-Voltage (I-V) Measurements

Poly(3,4-ethylene-dioxythiophene) doped with poly(styrenesulfonate) (also known as PEDOT-PSS, PEDOT or PDOT) has been utilized as a hole injecting material in OLEDs for some time [74]. While having a high work-function of ~5.1eV, PEDOT-PSS provides reduced hole injection barriers (about 0.2eV) into the HOMO energy level of numerous conjugated polymers, thus serving as a pseudo-ohmic contact to ITO anodes. In addition to these properties, PEDOT-PSS is commonly referred to as an organic metal since it exhibits ohmic transport similar to inorganic metals (Figure. 4-5).

"Hole-only", or more realistically "hole-dominated" devices, as described in Chapter 2, were prepared by evaporating gold electrodes onto the masked surface of two layer polymer films consisting of an active layer over the PEDOT-PSS layer. The samples were then placed in the sample holder (Figure 3-2) to measure I-V characteristics at room temperature. Voltage was ramped between 0 to 5 Volts (V), stepped by 0.05V, to provide several data points for curve-fitting. As depicted in Fig. 4-6, I-V data from a PProH device show exponential behavior similar to that of other conjugated polymers reported in the literature [36, 64, 75].

The I-V data for PProH films depended on the thickness as predicted by the space charge Equation, which shows that current is inversely proportional to thickness cubed (i.e., $J \alpha d^{-3}$). This dependence is qualitatively consistent with the PProH data presented in Fig. 4-7 in that the current is dramatically larger for the thinner layers. Note that at < 0.5V, the films maintain similar current density values, but the thinner 21nm film exhibited much higher currents at higher voltages. Additionally, the 88nm film exhibits the lowest currents for all voltages over the entire voltage range.

Since the space charge model shows that current-density is proportional to the square of applied voltage (i.e., $J \alpha V^2$), a plot of log J vs log V should result in a line having a slope of 2. Figure 4-8 shows shows such plots of the data presented in Figure 4-7.

A linear regression analysis of the data (Fig. 4-8) reveals that the slopes are best fitted by values of 2.1, 1.7 and 1.9 for 21, 44 and 88nm thick films, respectively. An average slope of 2 is indicative of space charge limited current, in contrast to materials which exhibit trap-limited-currents that show different slopes (i.e., $I \alpha V^m$ with $m > 2$). For example, if the log I vs. log V data were trap limited, a slope of three or higher would be expected [76]. This is due to a significant number of carriers injected from the electrodes being held at traps distributed in energy between the LUMO and HOMO energy levels of the polymer [77].

Plots log I versus log V for samples of ProDOT films are presented in Figure 4-9. The data for these films are consistent with trapped charge limited current (TCLC), rather than the SCLC behavior of PProH films. Trap limited current is indicated by the fact that $I \alpha V^3$ as linear regression results in a slope of 3.7 and 3.1 for the 25 and 47nm films.

It is not understood why ProDOT films exhibit TCLC while PProH films exhibit SCLC. However, in some material/solvent combinations there may be impurities remaining after synthesis of organic semiconductor materials and/or layers that could trap charges. Alternatively, the traps may be the result of structural disorder of the polymer films [78]. Structural disorder, resulting in defects, introduces localized energy levels between the HOMO and LUMO of the organic material which may be present as discrete energy levels, or distributed over a band of energy with a constant density of states or an exponential distribution such as a Gaussian. One other source of traps occurs when a charge carrier causes deformation of the organic molecule. In this case, the deformation acts as a quasi-particle called a polaron which not only has a lower mobility than a free carrier but also forms its own trap state in the polymer ("self trapping") [79]. Because some of the device preparation and testing steps were outside the glove box, there also remains the possibility that films and polymer solutions were contaminated by external impurities during processing. Further investigation is needed to understand why ProDOT exhibits trap limited while PProH exhibits space charge limited current transport.

To address the possibility that structural disorder and/or retained solvent was the source of traps the devices were heated so as to allow the polymers to rearrange. While still in the glove-box, the devices were placed on a hot plate and heated ("baked") to approximately 100^{o}C for ~4 hours. Upon removal from the hot-plate, the samples were allowed to cool for 30 minutes at which time I-V measurements were again performed. Increased currents were observed for the 25nm and 47nm films (Figure 4-10).

However, current-voltage measurements were again taken after an additional 15 hours of relaxation in room temperature argon ambient and the current decreased to

nearly the same values as before the baking (Figure 4-11).

These results suggest that the traps are not related to defects or solvents that are healed or reduced at ~100^{o}C heat treatments., Further experiments are needed.

4.2.2.2 Hole Mobility Analysis

Data for the hole mobility of P3HT and PProH films were analyzed based on the space charge model (Equation 2-19), solving for fitting parameters representing constants in the formula. The fitting parameters were calculated by iterating the field-dependent mobility equation (Equation 2-20) for the zero-field mobility, $\mu(0)$, and the field-dependence factor, γ, as presented in equation. The results are presented in Table 4.3 for the fitting parameters where the goodness of fit parameter, R^2, aproaching a value of one represents an excellent fit to the space charge model.

Data fitting for P3HT yields $\mu(o)$ values averaging $6.95 \pm 1.2 \times 10^{-6}$ (cm^2/V-s) with no thickness dependence, while that for PPrOH yields $\mu(o)$ values averaging $1.6 \pm 0.4 \times 10^{-6}$ (cm^2/V-s). The hole mobilities for various conjugated polymers as reported in the literature are listed in Table 4-4.

Based on the data in Table 4.4, the hole mobilities reported for PProH are similar to those reported for other conjugated polymers such as PPV [63, 80, 81]. However, the hole mobilities reported for P3HT are about two orders of magnitude smaller than those reported by Goh and Kline using a similar technique [36]. The reason is unknown. It was not possible to fit the TCLC model to the ProDOT I-V data to extract the hole mobility.

Table 4-1. Chemical Structure of sample polymers

Polymer Name	Structure
P3HT: RR-poly(3-hexyl-thiophene)	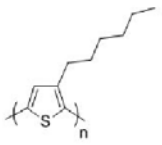
PProDOT: poly(3,4-propylenedioxythiophene)	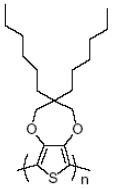
PProH: poly(3,4-propylenedioxythiophene-diethylhexyloxy)-cyano-p-phenylene vinylene(substituted with dodecyloxy chains on the phenylene ring)	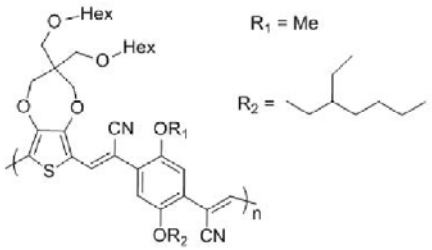

Figure 4-1. Depiction of channel formation for measurement of PEDOT-PSS film thickness

Figure 4-2. Depiction of channel formation for measurement of total film thickness

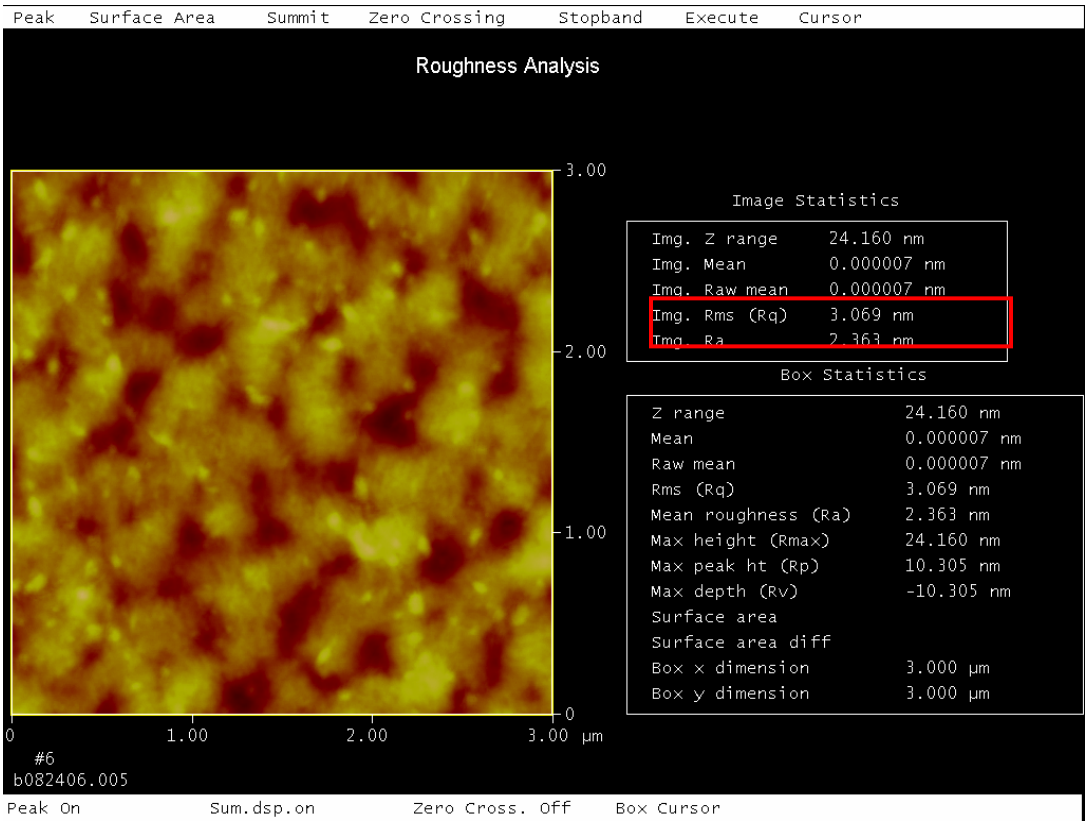

Figure 4-3. Typical AFM surface roughness analysis output with the RMS surface roughness in the red box

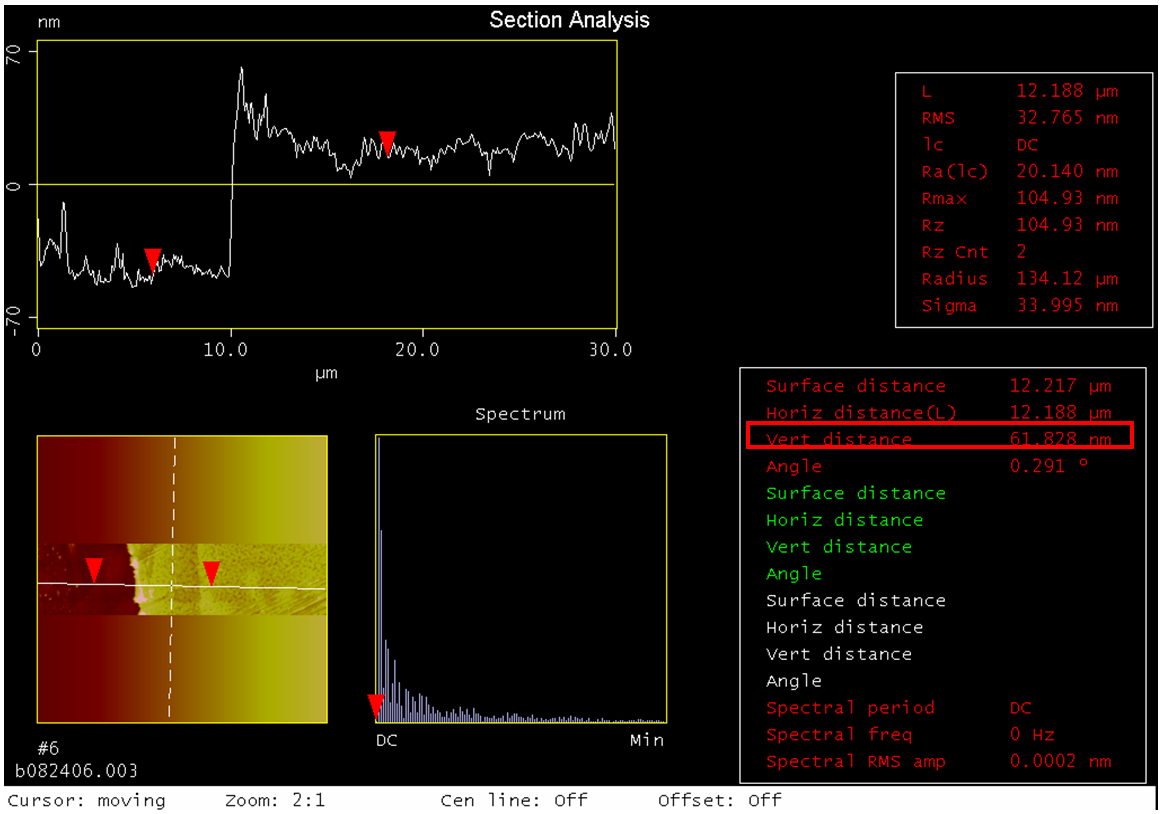

Figure 4-4. Depiction of film thickness measurements. The red arrows appear to the right and left of a channel wall.produced by scratching

Table 4.2. Thickness and RMS roughness data for all conjugated polymer films

Material	Sample ID	Solvent	Concentration (mg/mL)	Spin Rate (rpm)	Thickness (nm)	RMS (nm)
PEDOT	P	DI-Water	as received	3500	40	N/A
P3HT	Dev 3	di-chloroBenzene	20	1000	143	3.47
	Dev 4	di-chloroBenzene	20	800	148	4.39
ProDOT	A5	Toluene	~8 - 10	1000	25	0.85
	A6	Toluene	~8 - 10	900	47	3.17
PProH	6	di-chloroBenzene	8	1000	22	3.07
	B3	Toluene	28	900	44	5.14
	B4	Toluene	28	700	88	3.73

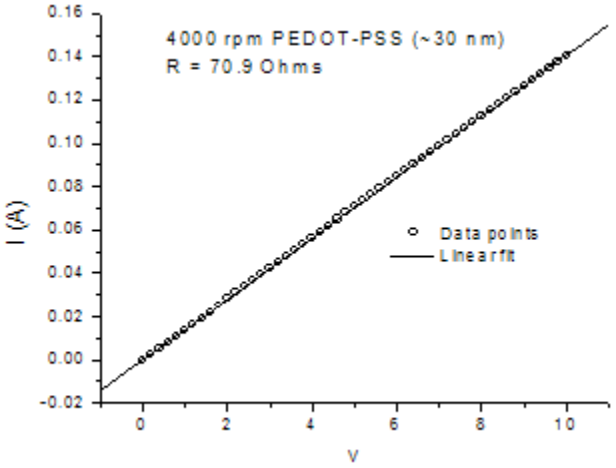

Figure 4-5. I-V data for PEDOT:PSS.

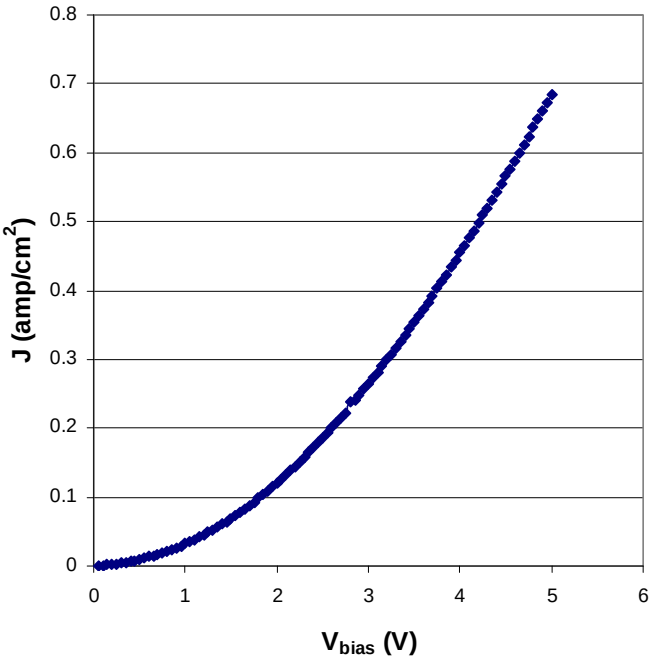

Figure 4-6. Typical J-V data for a PProH polymer device. Note the exponential character typical of polymer films.

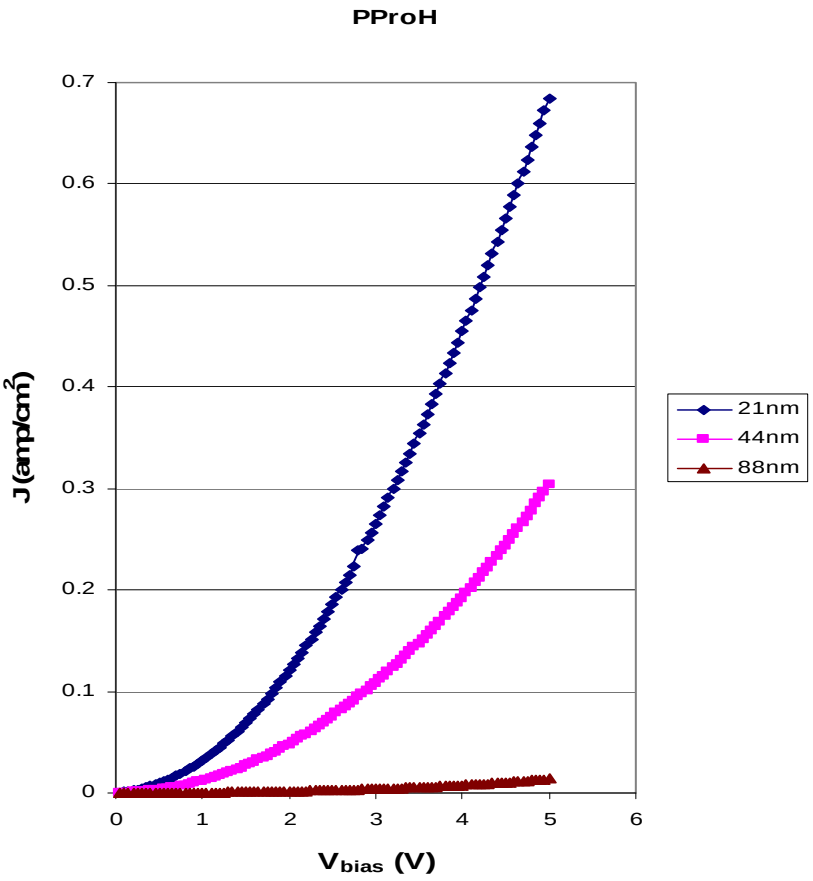

Figure 4-7. Dependence of J-V data on thickness for PPrOH films

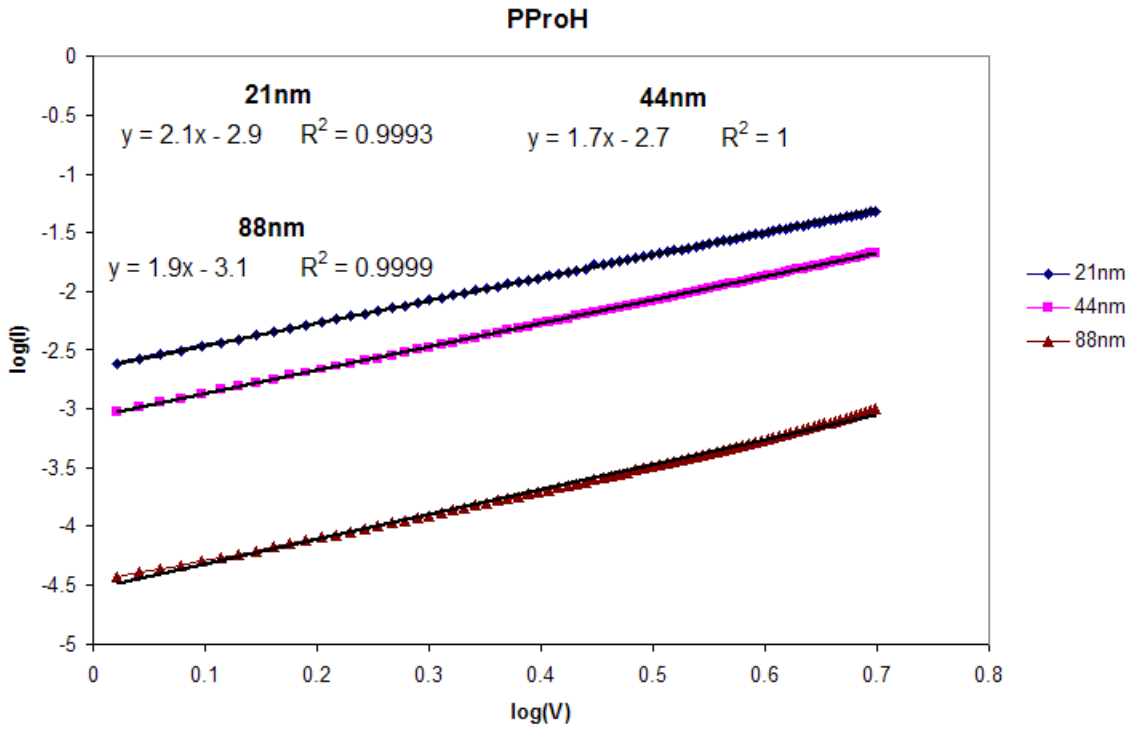

Fig. 4-8. Linear regression of log I vs log V data for PProH films. The slope = 2 suggesting that the data are described by the space charge limited current (SCLC) model

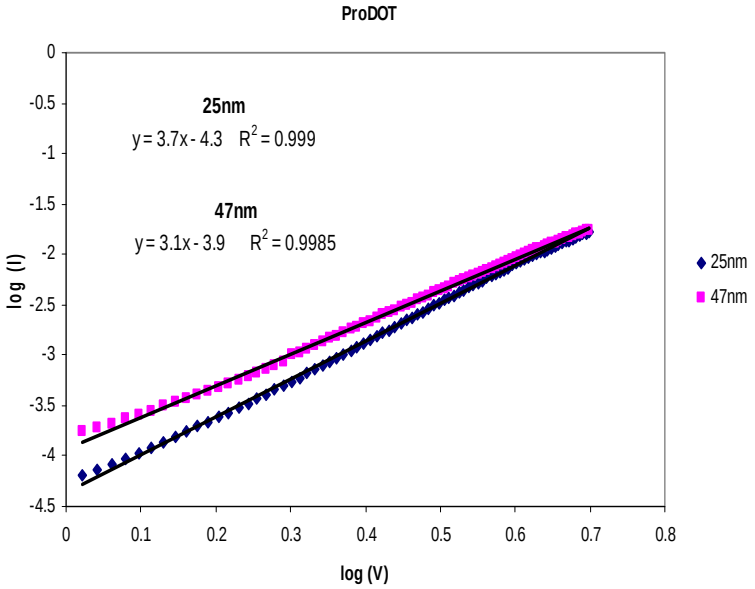

Figure. 4-9. Linear regression of log I vs log V data for ProDOT. The slope > 3 indicates TCLC

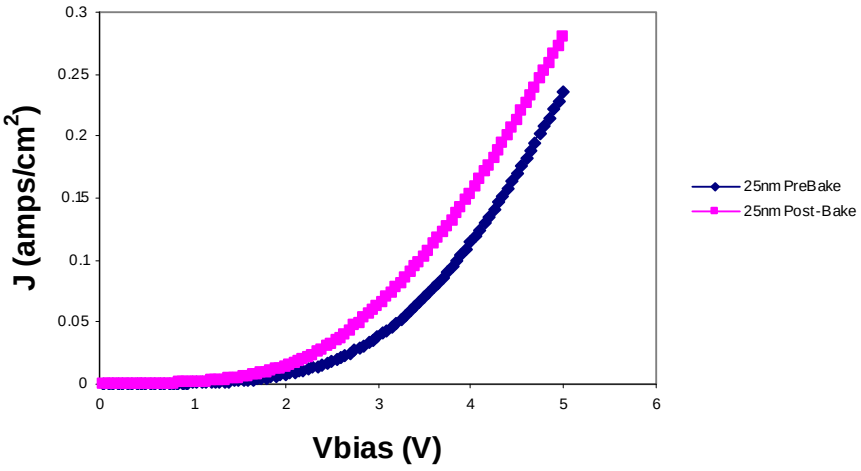

Figure 4-10. Increased J were observed upon heating the 25nm PProDOT samples

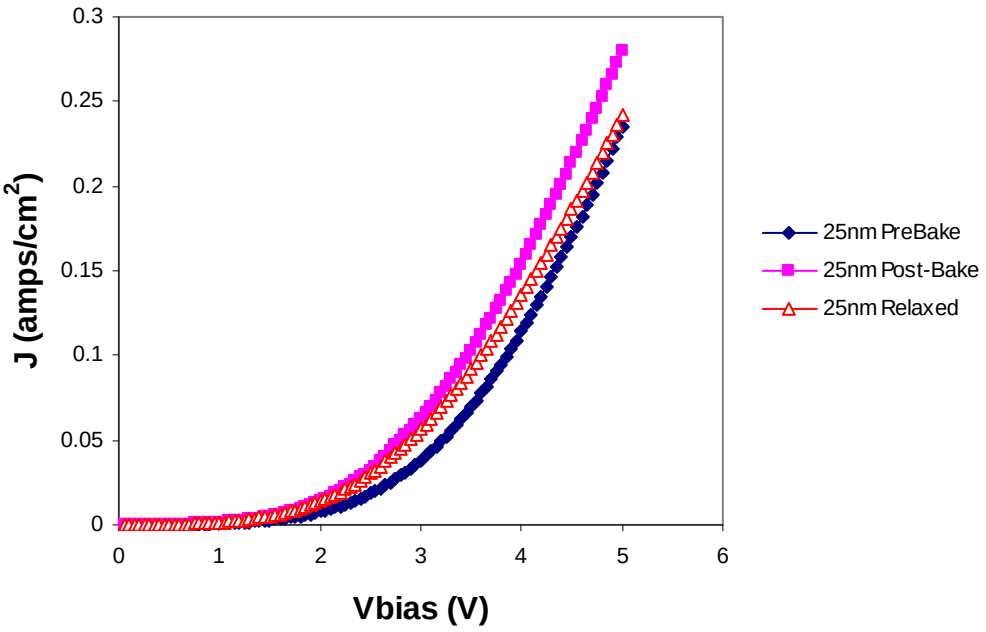

Figure 4-11. Effect of baking and relaxation on current density.

Table 4.3. Fitting parameters obtained by iterating the field-dependent mobility equation

Material	Sample ID	Thickness (nm)	μ(o) (cm^2/ V s)	□ (m/V)$^{1/2}$	R^2
P3HT	Dev 3	143	7.8 x 10^{-6} +/- 2.5	2.0 x 10^{-4} +/- 0.5	.9991
	Dev 4	148	6.1 x 10^{-6} +/- 1.1	1.2 x 10^{-4} +/- 0.6	.9997
PProH	6	21	1.4 x 10^{-6} +/- 0.2	2.6 x $10^{\wedge-5}$ +/- 1.0	.9999
	B3	44	3.3 x 10^{-6} +/- 0.5	8.6 x $10^{\wedge-6}$ +/- 6.0	.99996
	B4	88	9.4 x 10^{-8} +/- 0.2	2.6 x $10^{\wedge-4}$ +/- 0.2	.99984

Table 4.4. Hole mobilities of various polymers

Material	Mobility ($cm^2/V\ s$)	Method	Ref #
P3HT	4×10^{-4}	Time of Flight	[41]
AsF5 doped polyacetylene	2×10^{-2}	Van der Pauw	[54]
phenyl-amino subst. PPV	10^{-4} - 10^{-3}	Time of Flight	[44]
P3HT	1.3×10^{-5}	J vs V (SCLC)	[36]
PPV	0.5×10^{-6}	J vs V (SCLC)	[64]
poly(phenylene) Derivative	$\sim 10^{-6}$	J vs V (SCLC)	[65]
PPV (Spin cast)	0.8×10^{-6}	Time of Flight	[80]
poly (9,9-dioctylfluorene)	4.5×10^{-2}	Time of Flight	[82]

CHAPTER 5
CONCLUSION

The electrical properties of thin films of poly(3-hexyl-thiophene) ("P3HT"), poly(3,4-propylenedioxythiophene) ("PProDOT") and poly(3,4-propylenedioxythiophene-diethylhexyloxy)-cyano-p-phenylenevinylene substituted with dodecyloxy chains on the phenylene ring ("PProH") have been studied at various film thicknesses (<150nm). The focus was the use of current-voltage (I-V) data to determine if the transported current was space charge limited (SCLC) or trapped charge limited (TCLC). If the SCLC model applied, the hole mobilities was extracted from the data.

For PProH and P3HT, hole transport was described by the SCLC model with hole mobilities of $1.6 \pm 0.4 \times 10^{-6}$ and $6.95 \pm 1.2 \times 10^{-6}$ (cm^2/V-s), respectively. While the mobilities for P3HT are approximately two orders of magnitude lower than those previously reported in the literature, it is speculated that the larger thickness of the films (~143nm and ~148nm) may have contributed to lower mobilities, as well as a dependence of mobility upon the field strength for lower-molecular weight films [36].

In contrast, the I-V data from PProDOT fit the TCLC model in which $J \alpha V^m$ with values of m between 3 and 4. Heat treatment of the spin cast films to temperatures of 100^oC did not significantly change the I-V data and dependence of J upon V^m, suggesting that the traps were stable to these temperatures.

Future Work. While the method for characterizing the electrical properties of conjugated polymers can be used to measure the mobilities of materials exhibiting space charge limited currents (PProH and P3HT), it is difficult to measure the mobility for

trapped charge limited current, as for PProDOT. Knowledge of the trap distribution and density are required, that could be provided by a technique known as thermally stimulated currents (TSC) which has been used to measure trap levels and total density in poly(p-phenylenevinylene) ("PPV") [83]. While devices are cooled down from room temperature to as low as 10^{o}K, they are exposed to a strong forward bias, which fills all of the traps [84]. For a specific trap, there is an associated transport energy, or escape energy (i.e., the level from which a trapped carrier is most likely to be released) that is dependent on temperature. A trap state at lower temperatures may therefore become a transport state at room temperature [85]. Upon removing the electric field at the low temperature, the samples are allowed to reach an equilibrium thermal state at a higher temperature by thermal release of carriers from the traps into the bands. The thermally stimulated current rises as the temperature is increased and the results may be interpreted by correlating distinct current maxima with a distinct trap energy level by $I \alpha \exp(-E_t/kT)$ for $T< T_{max}$ [86]. This technique has been shown to provide good results for devices with conjugated polymers as the active layer [87].

Additionally, the method of measuring hole mobility was hindered by assumptions made in calculating the film thickness (d) which contributes to the space charge model as $J \alpha d^{-3}$. Although spin coating is quite often used as a reliable method for producing thin films, results are not always consistent as they depend on solution viscosity which depends on the material and solvent used. While a substrate cleaning procedure was followed and all solutions were filtered, the spin-cast polymer films often showed signs of non-uniform thickness, including holes, streaks and even particulates. Also, one of the challenges in this study was to repeat previous processing parameters in order to measure

repeatability of the I-V data. Specifically with PPrOH, the total amount of conjugated polymer was quite limited, making it difficult to a wide processing parameter field. Further investigation into optimizing device fabrication procedures for these materials would lead to more in depth-studies of the effects of film thickness on I-V measurements.

This study focused on measuring hole-mobilities, which are generally higher than electron-mobilities in conjugated polymer organic semiconductors. However, knowledge of the electron-transport properties must be acquired to further understand and optimize the properties of double carrier devices such as organic light emitting diodes. For example, to investigate the transport of electrons in PPV without the drawbacks of highly reactive Ca and Ba low-work function electrodes, Mandoc et al. constructed electron-only devices by vapor depositing alternative low work function, hole blocking materials as the electrodes. Utilizing a sandwich configuration with aluminum (Al) as the bottom electrode, ytterbium (Yb) as the top electrode and the active material between the electrodes, Mandoc was able to suppress hole injection at fields up to 10^8 V/m and measured an exponential distribution of electron-traps in PPV [87].

LIST OF REFERENCES

1. Conti, J., Annual Energy Outlook 2006 with Predictions to 2030, Energy Information Administration, Department of Energy DOE/EIA-0383, Washington DC, 2006.

2. Stolka, M., Organic Light Emitting Diodes (OLEDs) for General Illumination Update 2002, OptoElectronics Industry Development Association, Washington DC, 2002.

3. Eden, J.G., Proceedings of the IEEE 94 (2006) 567-574.

4. Crawford, G.P., Flexible Flat Panel Displays, John Wiley & Sons, West Sussex,England, 2005.

5. Kelly, S.M., "Flat Panel Displays Advanced Organic Materials, The Royal Society of Chemistry, Cambridge, UK 2000.

6. Mitschke, U., Bauerle, P., *J. Mater. Chem.*, 10 (2000) 1471-1507.

7. Loebner, E.E., *IEEE Transactions on Electron Devices*, 23 (1976) 675-699.

8. Zheludev, N., *Nature Photonics*, 1 (2007) 189-192.

9. Tang, C.W., VanSlyke, S.A., Appl. Phys. Lett. 51 (1987) 913-915.

10. Burroughes, J.H., Nature, 347(1990) 539-514.

11. Friend, R.H., Synth. Met., 84 (1997) 455-462.

12. Grice, A.W., Appl. Phys. Lett., 73 (1998) 629-631

13. Xu, Q., Appl. Phys. Lett., 83 (2003) 465.

14. Hamada, Y., Appl. Phys. Lett., 75 (1999) 1682 – 1684.

15. Yang, Y., Heeger, J., Appl. Phys. Lett., 64 (1994) 1245-1247

16. deKok, M.M., Phys. Stat. Sol., 201 (2004) 1342-1359.

17. Service, R. F., Science, 310 (2005) 1762-1763.

18. Bergh, A., Phys. Today, 54 (2001) 42-47.

19. Petrucci, R.H., Harwood, W.S., General Chemistry Principles and Modern Applications, sixth ed., Macmillan Publishing Company, New York, 1993.

20. Wade Jr., L.G., Organic Chemistry, third ed., Prentice Hall, New Jersey, 1995.

21. Kao, K.C., Hwang, W., Electrical Transport in Solids with Particular Reference to Organic Semiconductors, Pergamon Press, New York, 1981.

22. Kelsall, R., Hamley, I., Geoghegan, M., Nanoscale Science and Technology, John Wiley & Sons, Ltd., England, 2005.

23. Krutmeijer, E., Nordén, B., "The Nobel Prize in Chemistry, 2000: Conductive Polymers (Advanced Information)", Nobel Prize Foundation website http://nobelprize.org/nobel_prizes/chemistry/laureates/2000/chemadv.pdf)

24. Kasap, S. O., Principles of Electronic Materials and Device, second ed., McGraw-Hill Higher Education, New York, 2002.

25. McKelvey, J. P., Solid State Physics for Engineering and Materials Science, Krieger Publishing Company, Florida, 1993.

26. Tang, J., J. Mater. Chem. 13 (2003) 232-234.

27. Thienpont, H., Phys. Rev. Lett. (1990) 2141-2144.

28. Stone, D.A., J. Poly. Sci. A: Pol. Chem. 44 (2006) 69-76.

29. Kallitsis, J.K., Macromolecules, 30 (1997) 2989-2996.

30. Shaw, J. M., Seidler, P.P., IBM J. Res. & Dev, 45 (2001) 3-10.

31. Forrest, S.R., Adv. Mater. 15 (2003) 1043-1048.

32. Jabbour, G.E., Appl. Phys. Lett., 71 (1997) 1762-1764.

33. Bernius, M.T., Adv. Mater., 12 (2000) 1737-1750.

34. Pribat, D., Thin Solid Films, 383 (2001) 25-30.

35. Hummel, R., Electronic Properties of Materials, third ed., Springer, New York, 2001.

36. Goh, C., Appl. Phys. Lett., 86 (2005) 122110-2.

37. Parker, I.D., J. Appl. Phys. 75 (1994) 1656-1666.

38. Li, Z., Meng, H., Organic Light-Emitting Materials and Devices, CRC Press Taylor & Francis Group, Boca Raton Fl, 2007.

39. Ma, D., Solid State Communications 112 (1999) 251-254.

40. Sze, S.M., Physics of Semiconductor Devices, second ed., John Wiley & Sons, Inc., New York, 1981.

41. Kaneto, K., Jpn. J. Appl. Phys. Part 2 – Letters, 38, (1999) L1188-L1190.

42. Rubin, M., *Appl. Phys. Lett.* 64 (1994) 64-66.

43. Camaioni, N., Appl. Phys. Lett., 73(1998) 253-255.

44. Hertel, D., *J. Chem. Phys.*, 110 (1999) 9214-9222.

45. H.C. F. Martens, Appl. Phys. Lett., 77 (2000) 2057-2059.

46. Pingree, L.S.C., *Appl. Phys. Lett.* 86 (2005) 073509.

47. Naber, R.C.G., *Organic Electronics*, **7** (2006) 132-136.

48. Karl, N., Synth. Met., 133-134 (2003) 649-657.

49. Poplavsky, D., So, F., *J. Appl. Phys.* 99 (2006) 033707.

50. Kumar, V., *J. Appl. Phys.*, 92 (2002) 7325-7329.

51. Van der Pauw, L.J., *Philips Research Reports*, 13 (1958) 1-9.

52. Geerts, W., *Solid State Electronics*, 39, (1996) 1289-1294.

53. Kline, R. J., J. of Macromol. Sci., Part C: Polymer Reviews, 46 (2006) 27-45.

54. Seeger, K., Solid State Communications. 28 1978 837

55. Bos, F.C., *Phys. Rev. Lett.*, 58 (1987) 152-155.

56. West, D.P, *Chemical Physical Letters*, 326.(2000) 407-412,

57. Lee, S.H., *J. Appl. Phys.*, 95 (2004) 3565-3568.

58. Kalinowski, J., Organic Light-Emitting Diodes Principles, Characteristics and Processes, Marcel Dekker Publishing. New York, NY. 2005.

59. Benvenho, A.R.V., *Materials Research*, 4 (2001.) 133-136.

60. Campbell, A.J., *Optical Materials*, 9 (1998) 114-119.

61. Murgatroyd, P.N., *J. Phys. D: Appl. Phys.*, 3 (1970) 151-156

62. Chiguvare, Z., J. Appl. Phys., 94 (2003) 23507.

63. Blom, P.W.M., *Phys. Rev. B*, 55 (1997) R656-R659.

64. Blom, P.W.M., *Appl. Phys. Lett.*, 68 (1996) 3308-3310.

65. Ma, D., *J. Phys D: Appl. Phys.*, 32 (1999) 2568-2572.

66. Smith, R.W., Physical Review, 97 (1955) 1531-1537.

67. Burrows, P.E., Appl. Phys. 79 (1996) 7991-8006.

68. Schmechel, R., Phys. Stat. Sol. (a) 201 (2004) 1215-1235.

69. Kim, J.S., Thin Solid Films, 445 (2003) 358-366.

70. Hall, D.B., Poly. Eng. & Sci., 38 (1998) 2039-2045.

71. Moons, E., J. Phys. C: Condens. Matter, 14 (2002) 12235-12260.

72. Laubender, J., Synth. Met. 111-112 (2000) 373-376.

73. Baytron® product information brochure. HC Starck, Inc. Newton, MA. http://www.hcstarck.de/medien/allgemein/downloads/baytron_CH8000_4083_web.pdf

74. Scott, J.C., Synthetic Metals 85 (1997) 1197-1200.

75. Bussac, M.N., Phys. Rev. B 55 (1997) 15587-15590.

76. Yang, H., H., Holloway, P.H., J. Phy.s Chem. B, 107 (2003) 9705-9710.

77. Burrows, P.E., Shen, Z., J. Appl. Phys., 79 (1996) 7991-8006.

78. Brüting, W., Organic Electronics, 2 (2001) 1-36.

79. Arif, M.A.I., "Raman Scattering Studies and Charge Transport in Polyfluorenes", University of Missouri-Columbia Electronic Thesis & Dissertation Archives 2007.

80. Chayet, H., Synthetic Metals, 84 (1997) 621-622.

81. Bozano, L., App. Phys. Lett. 74 (1999) 1132-1134.

82. Kreouzis, T., Phys. Rev. B. 73, (2006) 235201.

83. Meier, M., J. Appl. Phys., 84 (1998) 87-92.

84. Stallinga, P., Physica B, 273-274 (1999) 923-926.

85. Schmechel, R., Phys. Stat. Sol. (a), 201 (2004) 1215-1235.

86. Alagiriswamy, A.A, Synthetic Metals 116 (2001) 297-299.

87. Mandoc, M.M, Phys. Rev. B, 73 (2006) 155205.

BIOGRAPHICAL SKETCH

Bryan Wilson was born to Harold J. Wilson and Isabel H. Wilson in Panama City, Republic of Panama where he was preceded by his older sister, Natalie and older brother, Jonathan. From ages 1-7, Bryan resided with his family in the Panama Canal Zone neighborhood of Diablo. Upon relocating to Key Largo, Florida in 1985 and subsequently to Miami, Florida in 1986, Bryan attended school at Cutler Ridge Elementary, Cutler Ridge Middle School, graduating from Miami Southridge Senior High School. Bryan attended the undergraduate program at the University of Florida (UF), graduating in December of 2001 with a Bachelors of Science Degree in Chemical Engineering. For the three years following graduation from UF, Bryan worked as an engineer for A&N Corporation in Williston, Florida. At A&N, Bryan learned about the semiconductor industry and became interested in electronic materials. It was in the Fall of 2004 that he began his graduate studies in the Materials Science Department, again at the University of Florida where he gained a deeper interest in semiconducting polymers. Upon graduation with his Masters Degree, Bryan will continue his role as a Patent Examiner at the US Patent and Trademark Office in Alexandria, Virginia where he started his career in September of 2006.